Numerical Simulation of Forebody Vortices at High Angle of Attack and their Control Using Innovative Systems

Patrick CHAMPIGNY, Sébastien DECK, Pascal DENIS, Sonia MAGNIANT
ONERA, Applied Aerodynamics Department
BP72-29 av. de la Division Leclerc
F-92322 CHATILLON Cedex
FRANCE

E-Mail: Patrick.Champigny@onera.fr

ABSTRACT

The existence of asymmetric flows at high angle of attack around slender bodies of revolution has been known since the early 50's and many experimental studies were conducted in the 80's and 90's. The work presented here is devoted to the numerical simulation of such flows, and to their control using mechanical or fluidic devices. It was found that with RANS methods using classical turbulence models the flow remains symmetric at 45 degrees of incidence and, that only hybrid approach such that a DES (Detached Eddy Simulation) method can give an asymmetric flow organisation as observed during the experiment. Moreover, it is shown that with this kind of method the overall forces, as well as the pressure distributions are in a good agreement with the experimental data. The second part of this study deals with the efficiency of control devices. Two types of actuator, continuous or pulsed jets and Deployable Flow Effectors were considered. Both have proven their capability to force the asymmetry and to generate side forces and yawing moments.

1. INTRODUCTION

The continuous request for enhanced performance of missiles and aircraft leads to consider flights at very high angles of attack in which control is very difficult to perform. This is mainly due to the shedding of asymmetric vortices from the forebody, producing side force, yawing moment and rolling moment that are difficult to predict. The existence of asymmetric flows at high angle of attack around slender bodies of revolution has been known since the early 50's, and many experimental works were conducted in 80's and 90's. The objectives of these studies were firstly to quantify this phenomena, secondly to get finer knowledge of the flowfields, and finally to try to control them. Afterwards, improvements in numerical methods were so high that Navier Stokes computations have been used to give a better insight into these very complex flows.

The aim of this paper is to present recent calculations performed at ONERA using advanced numerical methods. In the first part, attempts have been made to reproduce the experimentally observed asymmetric flowfields. Reynolds Averaged Navier Stokes methods using classical turbulence models as well as a DES (Detached Eddy Simulation) method were evaluated on this test case. In the second part, several techniques for manipulating and controlling the forebody vortices have been considered, and many computations were performed in order to assess the efficiency of these control devices. Steady and pulsed jets, as well as deployed flow effectors have been simulated within this study.

Champigny, P.; Deck, S.; Denis, P.; Magniant, S. (2006) Numerical Simulation of Forebody Vortices at High Angle of Attack and their Control Using Innovative Systems. In *Innovative Missile Systems* (pp. 24-1 – 24-16). Meeting Proceedings RTO-MP-AVT-135, Paper 24. Neuilly-sur-Seine, France: RTO. Available from: http://www.rto.nato.int/abstracts.asp.

Report Documentation Page

Form Approved
OMB No. 0704-0188

1. REPORT DATE	2. REPORT TYPE	3. DATES COVERED
01 MAY 2006	**N/A**	**-**

4. TITLE AND SUBTITLE	5a. CONTRACT NUMBER
Numerical Simulation of Forebody Vortices at High Angle of Attack and their Control Using Innovative Systems (U)	5b. GRANT NUMBER
	5c. PROGRAM ELEMENT NUMBER
6. AUTHOR(S)	5d. PROJECT NUMBER
	5e. TASK NUMBER
	5f. WORK UNIT NUMBER
7. PERFORMING ORGANIZATION NAME(S) AND ADDRESS(ES) **ONERA, Applied Aerodynamics Department BP72-29 av. de la Division Leclerc F-92322 CHATILLON Cedex FRANCE**	8. PERFORMING ORGANIZATION REPORT NUMBER
9. SPONSORING/MONITORING AGENCY NAME(S) AND ADDRESS(ES)	10. SPONSOR/MONITOR'S ACRONYM(S)
	11. SPONSOR/MONITOR'S REPORT NUMBER(S)

12. DISTRIBUTION/AVAILABILITY STATEMENT
Approved for public release, distribution unlimited

13. SUPPLEMENTARY NOTES
See also ADM401233. RTO-MP-AVT-135, Presented at the RTO Applied Vehicle Technology Panel (AVT) Business Meeting Week in Amsterdam, the Netherlands, 15-18 May 2006., The original document contains color images.

14. ABSTRACT
See the report.

15. SUBJECT TERMS

16. SECURITY CLASSIFICATION OF:			17. LIMITATION OF ABSTRACT	18. NUMBER OF PAGES	19a. NAME OF RESPONSIBLE PERSON
a. REPORT	b. ABSTRACT	c. THIS PAGE			
unclassified - NATO	**unclassified**	**unclassified**	**SAR**	**49**	

Standard Form 298 (Rev. 8-98)
Prescribed by ANSI Std Z39-18

2. NUMERICAL SIMULATION AT HIGH ANGLE OF ATTACK

2.1. Test case

This study is focused on an ogive-cylinder fuselage at high angle of attack in low subsonic flow. Experiments were carried out in the pressurized wind tunnel F1 at ONERA Fauga-Mauzac center (near Toulouse) over a large range of angle of attack (0 to 80 degrees) and Reynolds number. The test section is rectangular and the dimensions of the test chamber are 4.5m×3.5m as can be seen in Figure 1. A detailed description of the experimental arrangement, equipment and results is given by Champigny [1].

The model consists basically of a 120mm diameter cylindrical body with a 3D tangent ogive nose. The model was equipped with 354 pressure taps whereas the aerodynamic loads were measured with a 6-component balance.

The present study concerns the conditions at 45 degree angle of attack where the Mach number is set to 0.2 and the Reynolds number, based on the free stream velocity and the diameter is equal to 2×10^6, conditions corresponding to a fully turbulent flow.

The grid used within this study is presented in Figure 2. The three-dimensional grid has been obtained by rotating a two-dimensional grid around the cylinder axis every 2 degree on the upper-side while an azimutal discretisation of 10 degrees is used on the lower side to limit the total number of grid points at 2.10^6 nodes. It is also worth noting that the base is not taken into account (infinite body).

2.2. Turbulence modelling

One of the objectives of this study is to assess the capability of several turbulence modelling to capture the asymmetrical vortical structure.

The RANS calculations are firstly based on the use of the Spalart-Allmaras model (SA) which solves a one-equation turbulence model for the eddy viscosity $\tilde{\upsilon}$:

$$\frac{D\tilde{\upsilon}}{Dt} = \underbrace{c_{b1}\tilde{S}\tilde{\upsilon}}_{production} + \underbrace{\frac{1}{\sigma}\left\{\nabla.\left[(\upsilon+\tilde{\upsilon})\nabla\tilde{\upsilon}\right]+c_{b2}(\nabla\tilde{\upsilon})^2\right\}}_{diffusion} - \underbrace{c_{w1}f_w\left(\frac{\tilde{\upsilon}}{d}\right)^2}_{destruction} \tag{1}$$

The eddy viscosity is defined by:

$$\mu_t = \rho\tilde{\upsilon}f_{v1} \qquad f_{v1} = \chi^3/\left(\chi^3+c_{v1}^3\right) \qquad \chi = \tilde{\upsilon}/\upsilon \tag{2}$$

and we refer to the original paper [6] for further details on the constants and the quantities involved. To get a better description of the vortical flow, a rotation correction (named SARC) which consists in modifying the production term by taking into account both the rate of strain and vorticity has also been evaluated (see Ref. [6]).

Furthermore, it seems to be generally accepted that the accurate prediction of massive separated flows is beyond the capabilities of classical URANS approaches. This comes mainly from the fact that dominant eddies in separated flows are highly specific of the geometry and do not have much in common with the standard eddies of the thin shear flows that classical RANS turbulence models are designed to model. Among hybrid strategies, the approach that has probably drawn most attention is the Detached Eddy Simulation (DES) which was proposed by Spalart et al. [5] in 1997. This method has given encouraging results for a wide range of flows exhibiting massive separation [6] [7] [8] [10] and has since gone through

various stages of refinement. The reader is referred to Spalart [9] for current status and perspectives in Detached Eddy Simulation. Nevertheless, let us recall the basic formulas of DES for the length scale $\tilde{d}$ that enters the turbulence model and controls the eddy viscosity:

$$\tilde{d} = \min(d, C_{DES}\Delta)$$

where d is the distance to the wall, C_{DES}=0.65 and $\Delta = \max(\Delta x, \Delta y, \Delta z)$ is the chosen measure of the grid spacing.

2.3. Numerical method

The current study has been performed with the FLU3M solver which solves the Navier-Stokes equations on structured multi-block grids. These equations are discretized using a second-order accurate upwind finite volume scheme and a cell-centered discretization. The solution is advanced in time using Gear's second order accurate implicit scheme. Further details concerning the numerical method and implementation of turbulence models can be found in [11] and [12].

2.4. Results and Discussions

Figure 3 displays the fields of eddy viscosity at location X/D=3.29. One can notice that the present RANS calculations with both SA and SARC models yield a perfect symmetric solution. It is also worth noting that the rotation correction decreases drastically the eddy viscosity in the core of the vortices (compared to the standard SA model) but does not modify the global symmetry of the solution. Unlike RANS calculations, the crossflow streamline pattern computed by DES clearly exhibits an asymmetric flow organisation but the topological structure of the flow in a crossflow plane remains the same as in the case of a corresponding symmetric flow. The DES calculation shows that fluid leaves the body along a surface of separation and rolls up behind the body to form a secondary vortex structure.

The computed and measured circumferential surface pressure distribution on different cross sections of the body is then given in Figure 4. This pressure coefficient is defined by:

$$C_p^* = \frac{P - P_0}{1/2\rho_0 V_0^2 \sin^2\alpha}$$

where α denotes the angle of attack and the subscript 0 refers to the free stream conditions.

In contrast to the symmetric behavior obtained using RANS calculations, the experimental pattern of the surface pressure distribution reflects the asymmetry of the flowfield. Indeed, one can notice the sign change of the asymmetry when going from the nose to the rear part which corresponds to the alternative shedding of the vortices on each side of the body (see Figure 5). The main features of this typical pressure distribution are well reproduced by the DES solution.

Finally, the integration of this pressure field able one to compute the streamwise evolution of the local force coefficient (see Figure 6). The local side force is defined by:

$$CY_{local} = \frac{1}{D}\int_0^{2\pi} \frac{P - P_0}{q_0 \sin^2\alpha} r \sin\theta \, d\theta$$

One can notice that the side force obtained with the present RANS calculations is zero since the flowfield remains perfectly symmetric, whereas the experimental local side force distribution is axially cyclic in

nature due to the alternative shedding of the vortices mentioned before,. This important feature of CY_{local} is well reproduced by the DES calculation. Nevertheless the coefficient obtained with DES is not damped when going to the rear-part unlike in the experiment. This may be due to the fact that the body has an infinite length in the calculations, and that no wall effects were considered. These points will be analyzed in the future as well as the possible unsteady effects related to the base.

3. CONTROL AT HIGH ANGLE OF ATTACK

The second objective of this study deals with the efficiency of control devices. As noticed in previous experimental and numerical studies [1], high angle of attack flows are very sensitive to small surface imperfections near the nose tip. Based on this assumption, several techniques for manipulating or controlling the forebody vortices have been considered.

For this study, the test case is the same as previously, excepted that the flow conditions have been changed to take into account future experiments. So, the main conditions are a freestream Mach number equal to 0.1, stagnation pressure and stagnation temperature values respectively equal to 1 bar and 288 K, leading to a Reynolds number of 0.94 10^5 (based on the body diameter). In view to these conditions, the flow is considered as laminar.

On the previous grid, a RANS computation at an angle of attack of 45 degrees has been performed with the FLU3M code. Classical numerical options are chosen (Roe flux, Minmod limiter,…) and about 20000 iterations are required to get the aerodynamic coefficients converged.

A view of the flowfield around the body is presented in Figure 7. In the present case, a perfectly symmetrical solution exhibiting no asymmetrical vortices is obtained. Rather than trying to find an asymmetrical solution by changing parameters, a large number of computations were carried out in order to assess the efficiency of jets or deployed flow effectors for the control of the flow.

3.1. Jet device

During this study, a simple, effective, efficient pneumatic method of forebody vortex asymmetry control has been evaluated. The jet technique uses the displacement effect of sight blowing to in fact reshape the forebody nose contour, thereby triggering the high angle of attack vortex configuration instability mechanism [13]. This action results in the control of vortex asymmetry and associated asymmetric forces.

Based on our knowledge on nose vortex control issued to previous wind tunnel tests [14], a configuration has been designed. So, two mirror holes with a 0.6 mm diameter, close to the nose (5 mm) and at azimuth angle of 115 degrees have been selected, as described in Figure 8. It is also worth noting that the injection is not in the normal wall direction but in the axial body axis, and forward.

In a first time, steady blowing has been simulated. The jet conditions are a Mach number close to 0.19 (V_{jet} ≈60 m/s), and the same stagnation pressure and temperature than the main flow. Then, the mass flow jet is 0.02 g/s which corresponds to a the momentum coefficient C_μ $\left(C\mu = \dot{m}_{jet} / \rho_\infty V_\infty S_{ref} \right)$ of 2.10^{-3}. It is important to appreciate the extremely low flow rates represented by the very small values of C_μ that are effective in blowing jet.

Figure 9 shows that, as expected, the vortex flow becomes asymmetric with a steady blowing in one of the holes (left one in this example). Moreover, one can notice that further downstream asymmetrical vortices are shed periodically, as presented in Figure 10 where the vortex sheets highlighted using the Q-criterion. Then, as a result, a side force is generated.

Starting with this asymmetrical case, a computation with a steady blowing from the other hole has been conducted to see if the vortex control is possible with this device. Then, a mirror solution is calculated and an opposite side force is obtained (Figure 11). This result confirms that the side force direction is depended on the blowing orifice.

After that, parametric studies were carried out. First of all, the jet characteristic effect was studied, especially the momentum coefficient C_μ. With a value divided by ten (corresponding to jet speed close to 20 m/s), a similar asymmetric flowfield is obtained but the side force created is weaker than before (Figure 12). So, this calculation clearly shows that the side force intensity can be modulated by this parameter. Then, the efficiency of this control device was investigated at 30 and 10 degrees. The results demonstrate that this concept is only valid over a limited angle of attack range, the vortex shedding at lower incidence being too stable to become asymmetric with a blowing jet (Figure 13).

Pulsed jet has been also simulated on this test case within this study. As our previous experiments have shown that the pulsed jet frequency is not the essential criteria for the control [14], one value was chosen (f=500 Hz), and during 33 and 17% of this period, an injection is effectively done. The Figure 14, where the results of these two cases are drawn, shows that an asymmetrical solution is obtained for both. Moreover, one can also observe that the side force intensity is depended on the duration of the injection. So, with this control device, it will be easy to modulate the induced forces.

3.2. Deployed Flow Effectors device

The second device evaluated within this study are the Deployed Flow Effectors (DFEs) [15]. DFEs are active micro-vortex generators that effectively disturb the flowfield along the forebody, yielding to large side forces and yawing moments for yaw control. The DFEs are small mechanical tabs with dimensions of 4 x 2 x 0.5 mm in our case, and placed underneath the surface in their retracted state (non-obtrusive to the flow). Upon controlled deployment, the DFEs interact with the forebody vortical flowfield to generate a desired yawing moment at high incidence. The considered forebody (described Figure 15) is equipped with two mirror deflectors, located close to the nose (less than half calibre) and at the same azimuth angle than the jet control (115 deg.). Moreover, the DFE height is varying from 0.5 to 2 mm.

To simplify the mesh, each DFE is considered without thickness and so, is introduced into a boundary condition in the initial mesh. Then, the efficiency of this device has been numerically investigated for the same flow conditions as previously and the main results are displayed in Figure 16. One can notice that the flow around the body has lost its symmetry with the left DFE is active. Indeed, this surface has led to asymmetric vortex detachment from the forebody, and this results in the generation of substantial opposite side force. As for the jet device, the results obtained with the right DFE deployment have demonstrated that the side force direction can also be controlled by combinations of both. Finally, some calculations have shown that the DFE span could allow controlling the intensity of this side force.

4. CONCLUSION

A numerical study was conducted with two main objectives. The first one was to verify the ability of numerical tools to predict the asymmetric character of the flows at high angles of attack, and the second one was to assess numerically the capability of specific devices to control these asymmetries and so the forces and moments. The main conclusions of this study are:

- RANS codes using classical turbulence models are not able to correctly simulate the asymmetric vortex shedding at high angle of attack;
- Hybrid methods like the DES approach have shown their ability to well reproduce the main flow features as well as the pressure distributions or the side forces;

- The control of flow asymmetry is possible using devices such as jets (continuous or pulsed) or Deployable Flow Effectors; their good efficiency comes from the fact that asymmetric flows are very sensitive to small disturbances near the nose tip;
- Nevertheless, their efficiency is limited to the high alpha range (i.e. greater than 30 degrees).

REFERENCES

[1] P. Champigny. "Reynolds number effect on the aerodynamic characteristics of an ogive cylinder at high angles of attack" *AIAA paper 84-2176, 1984.*

[2] P.R. Spalart, S.R. Allmaras. "A One-Equation turbulence model for aerodynamic flows" *La Recherche Aerospatiale, pp 5-21, 1994*

[3] J. Dacles-Mariani, G.G. Zilliac, J.S. Chow and P. Bradshaw. "Numerical/Experimental study of a Wingtip Vortex in the near field" *AIAA J., vol 33, No. 9, pp 1561-1568, 1995.*

[4] P. Sagaut. "Large-Eddy Simulation for Incompressible Flows" *Springer-Verlag; Berlin, 2002*

[5] P.R. Spalart, W.H. Jou, M. Strelets, and S.R., Allmaras. "Comments on the feasibility of LES for wings and on a hybrid RANS/LES approach" *In Proceedings pp 137-147, 1st AFSOR Int. Conf. on DNS, Ruston, 1998.*

[6] K.D. Squires, J.R. Forsythe, S.A. Morton, W.Z. Strang, K.E. Wurtzler, R.F. Tomarao, M.J. Grismer and P.R. Spalart. "Progress on Detached-Eddy Simulation of Massively Separated Flows" *AIAA paper 02-0591, Reno, Jan. 2002.*

[7] M. Strelets. "Detached Eddy Simulation of Massively Separated Flows" *AIAA paper 01-0879, Reno, Jan. 2001.*

[8] J.R. Forsythe, K.D. Squires, K.E. Wurtzler and P.R. Spalart. "Detached Eddy-Simulation of Fighter Aircraft at High_Alpha" *AIAA paper 02-0591, Reno, Jan. 2002.*

[9] P.R. Spalart. "Topics in Detached Eddy Simulation" *ICCFD3, Torronto, Canada, July, 2004.*

[10] S. Deck, E. Garnier and Ph. Guillen. "Turbulence modelling applied to space launcher configurations" *Journal of Turbulence, vol.3, (57), pp1-21, Dec. 2002*

[11] M. Péchier, P. Guillen and R. Cayzac. "Magnus Effect over Finned Projectiles" *Journal of Spacecraft and Rocket, Vol 38, No.4, pp542-549, 2001.*

[12] S. Deck, P. d'Espiney, Ph. Duveau, and Ph. Guillen. "Development and Application of Spalart Allmaras One Equation Turbulence Model to Three Dimensional Supersonic Complex Configurations" *Aerospace, Science and Technoloy, vol 6, no 3, pp 171-183, 2002.*

[13] F.W. Roos. "Microblowing : An effective, efficient method of vortex-asymmetry management" *AIAA paper 00-4416, Denver, Aug. 2000.*

[14] C. Francois. "Contrôle actif de l'écoulement autour d'une pointe avant à grande incidence" *RTO AVT Symposium on « Active Control Technology for Enhanced Performance Operational Capabilities of Military Aircraft, Land Vehicles and Sea Vehicles", Braunschweig, Germany, 8-11 May 2000*

[15] M.P. Patel, T.S.Prince, R.Carver and al. "Deployable flow effectors for phantom yaw control of missiles at high alpha" *AIAA paper 02-2827, St Louis, Missouri, Jun. 2002*

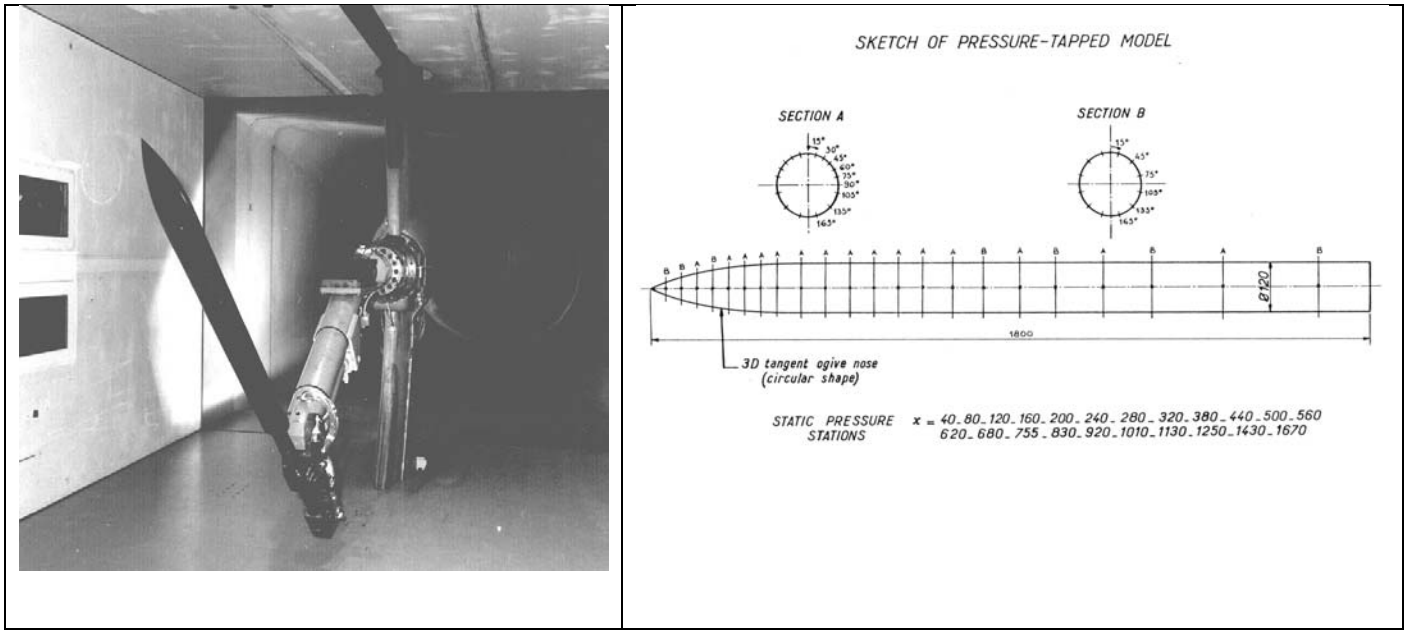

Figure 1 – Ogive-cylinder in the test section

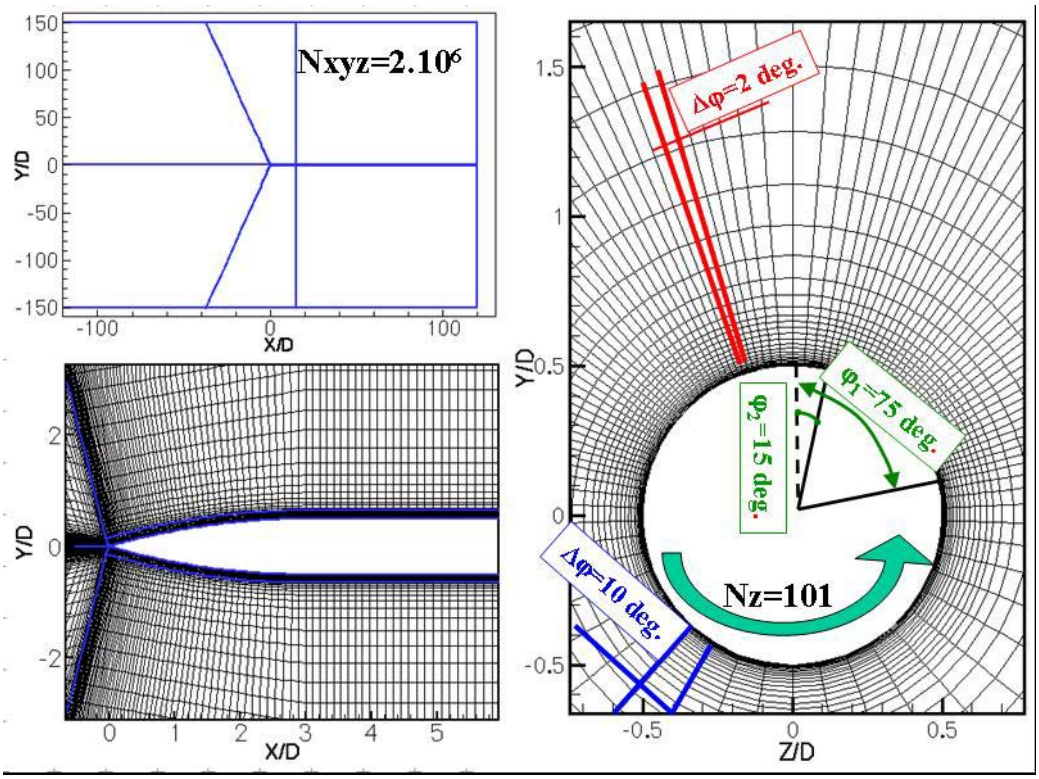

Figure 2 - Grid

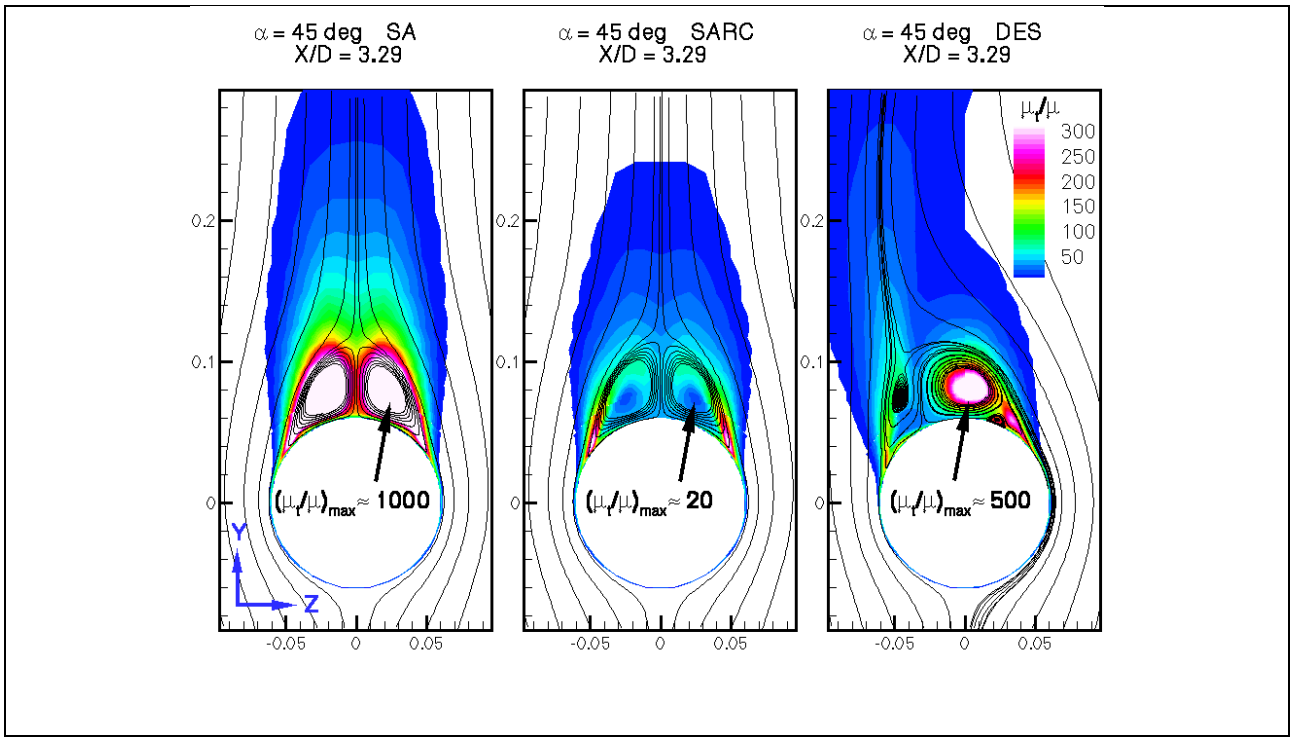

Figure 3 – Eddy viscosity fields

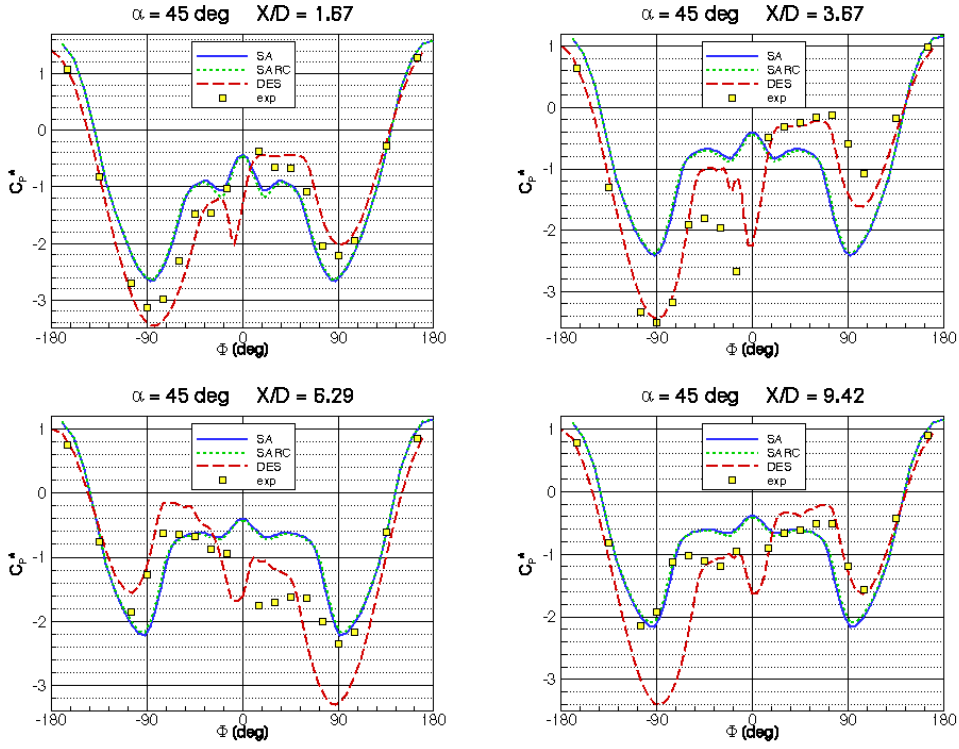

Figure 4 – Cp distribution

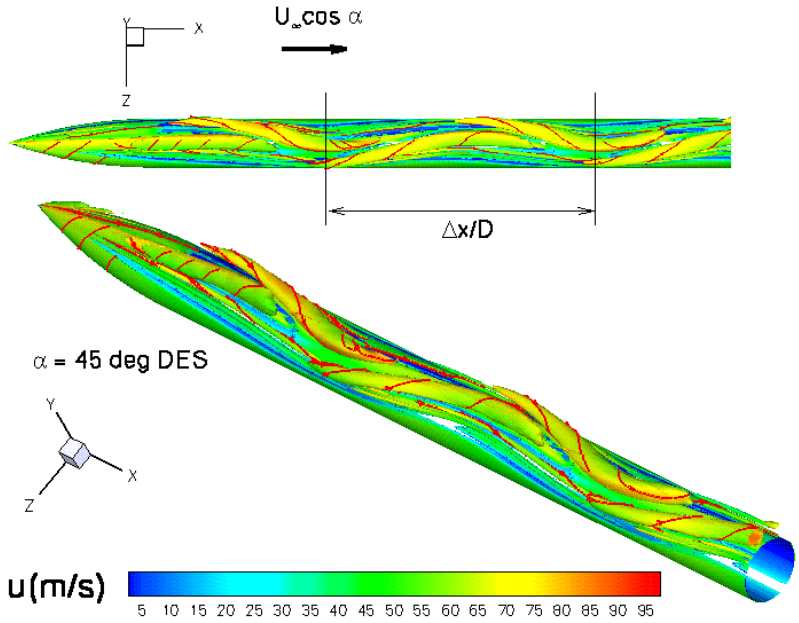

Figure 5 – Vortex sheet educed with the Q-criterion

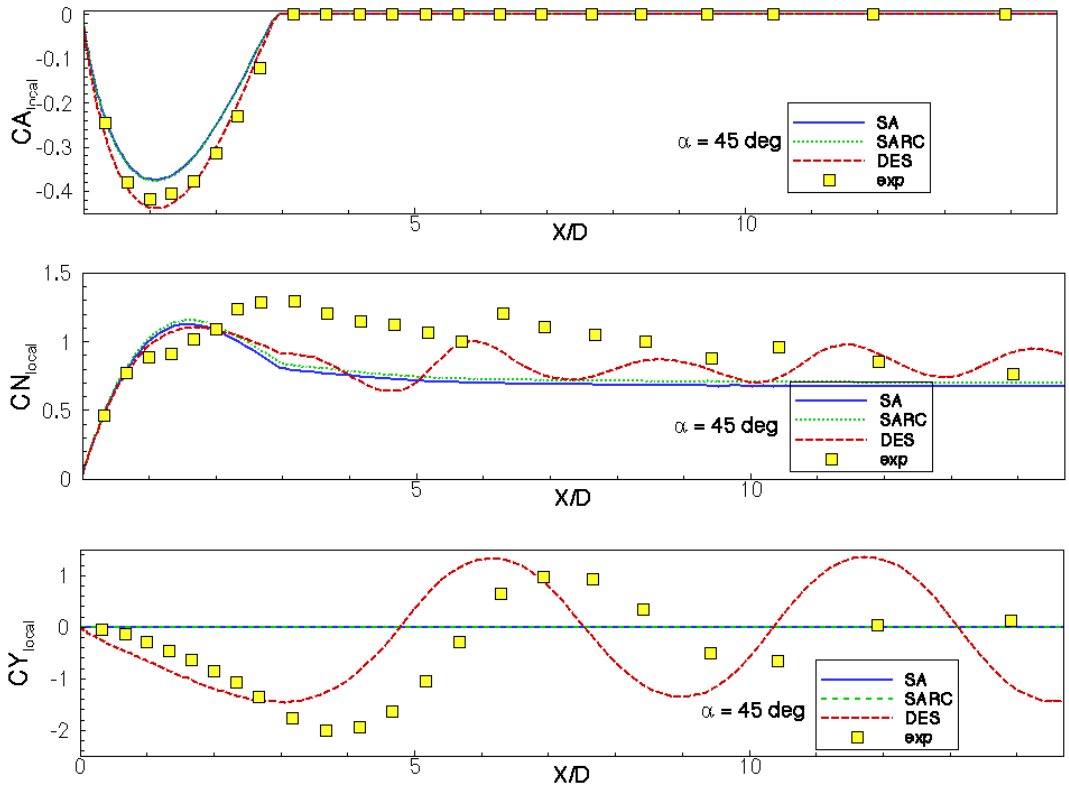

Figure 6 – Local force coefficient

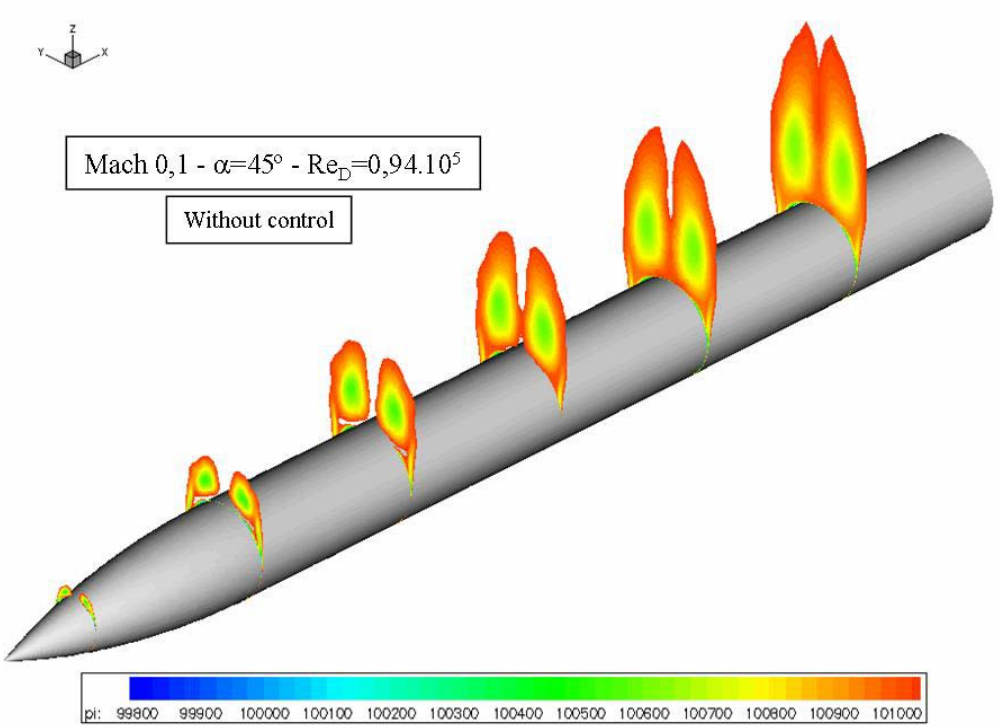

Figure 7 – Total pressure (without control)

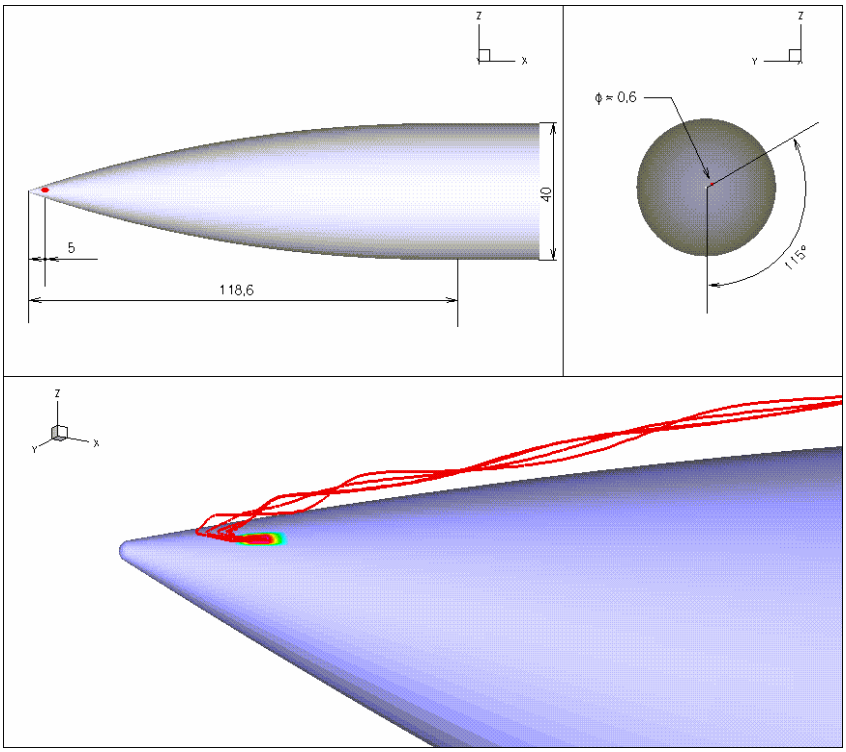

Figure 8 – Description of the jet device

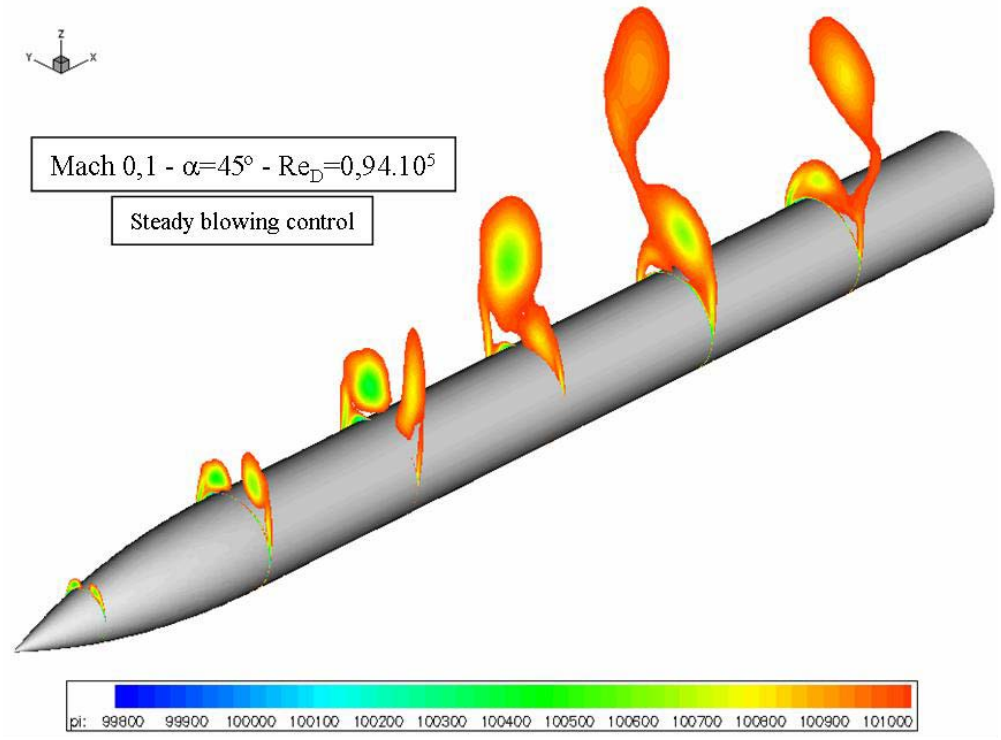

Figure 9 – Total pressure (with blowing control)

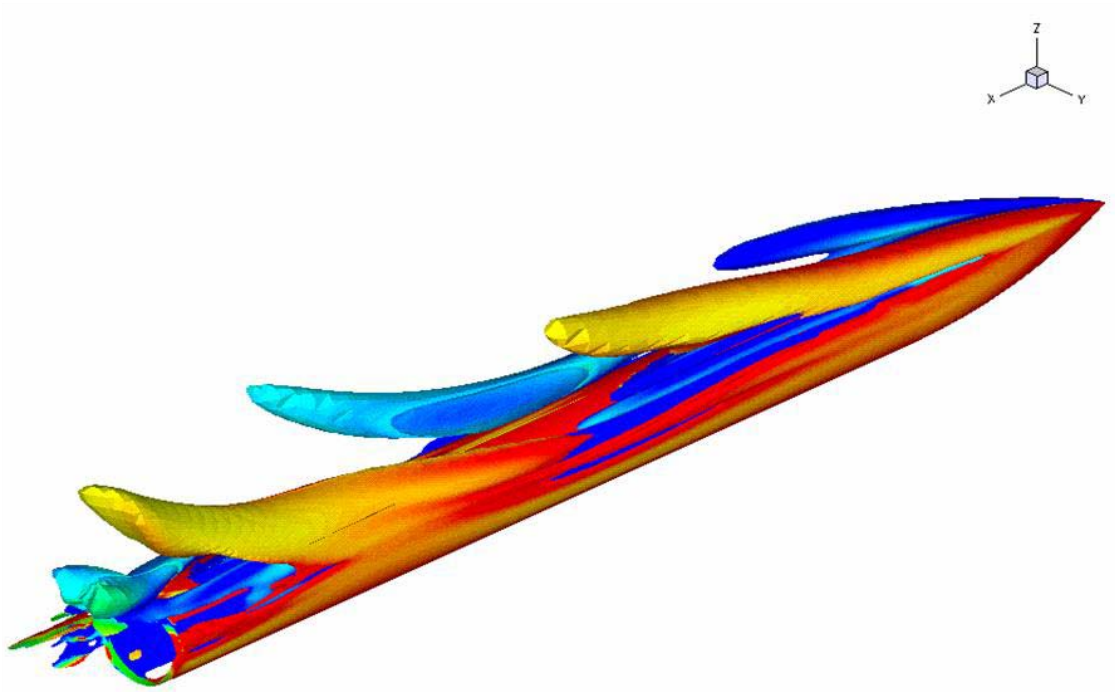

Figure 10 – Vortex sheet educed with the Q-criterion

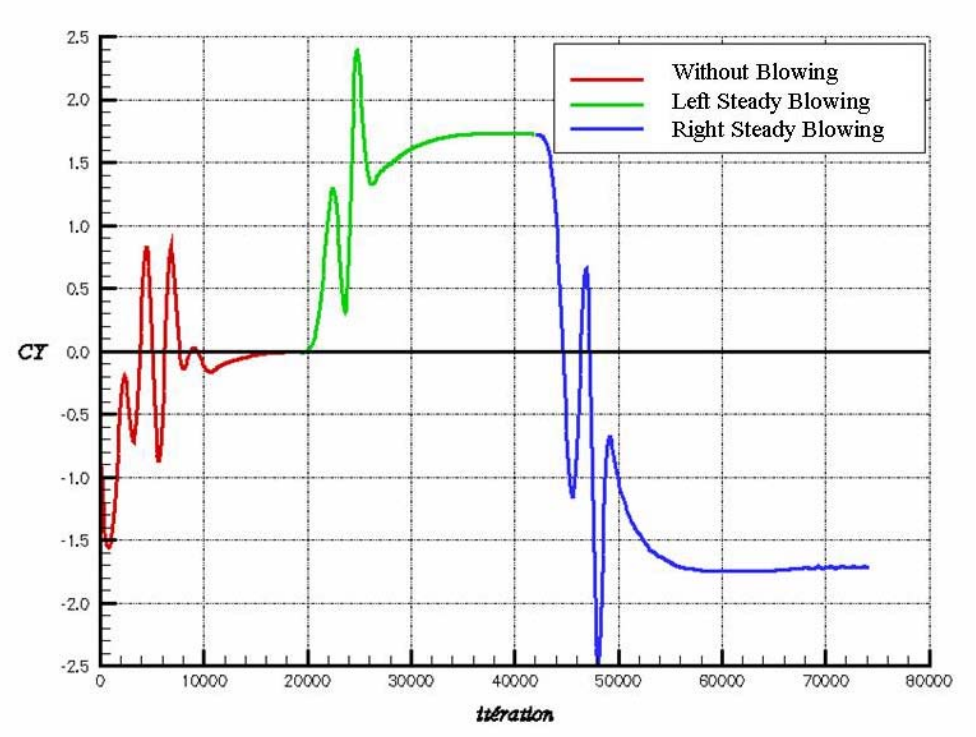

Figure 11 – Side force coefficient (steady blowing effect)

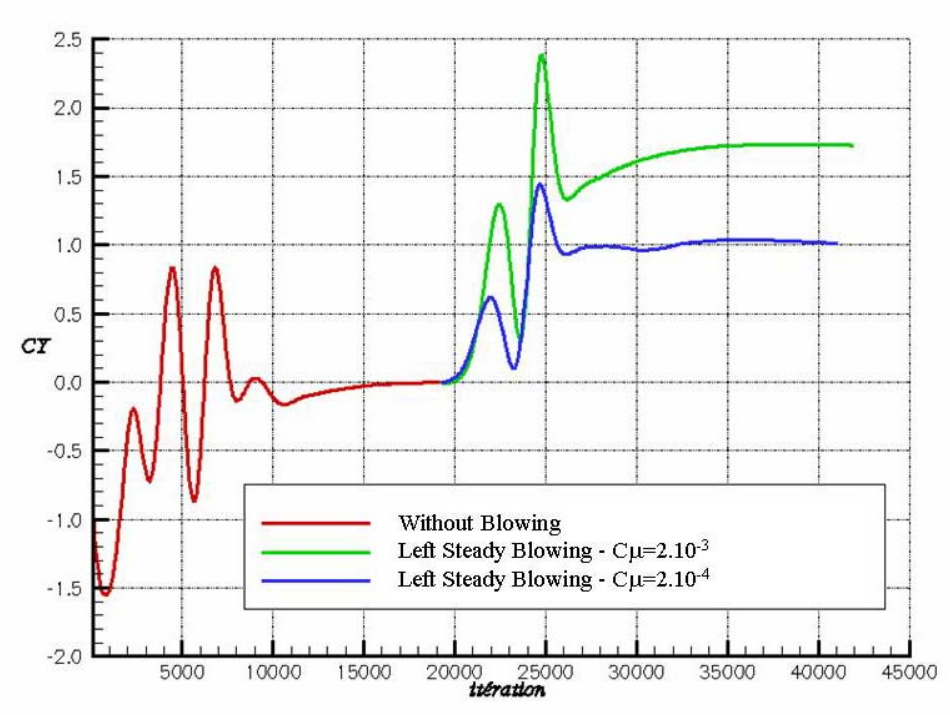

Figure 12 – Side force coefficient (momentum coefficient effect)

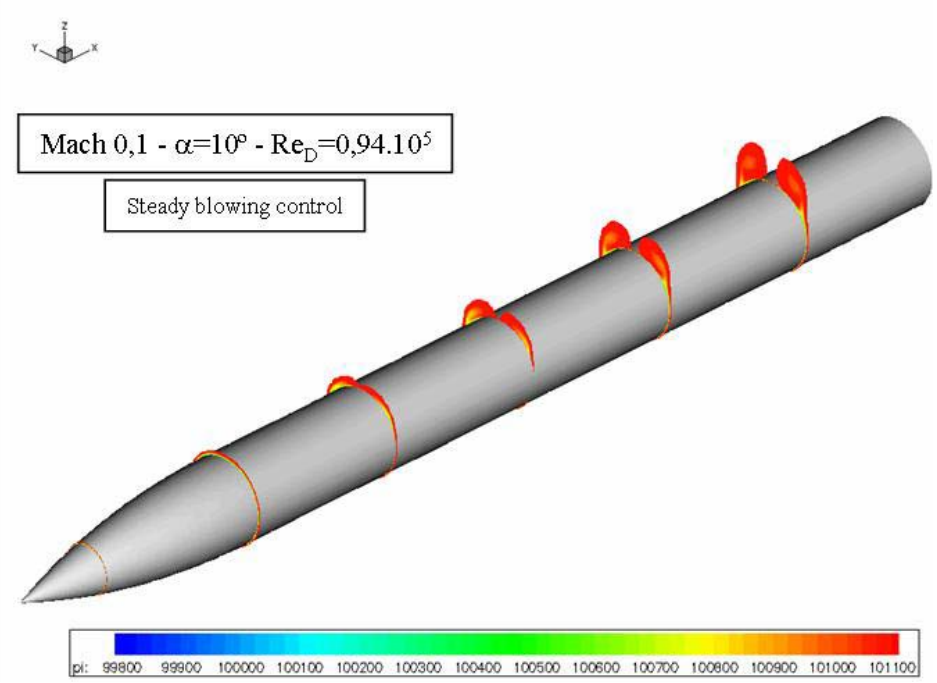

Figure 13 – Total pressure – α=10° – (with control)

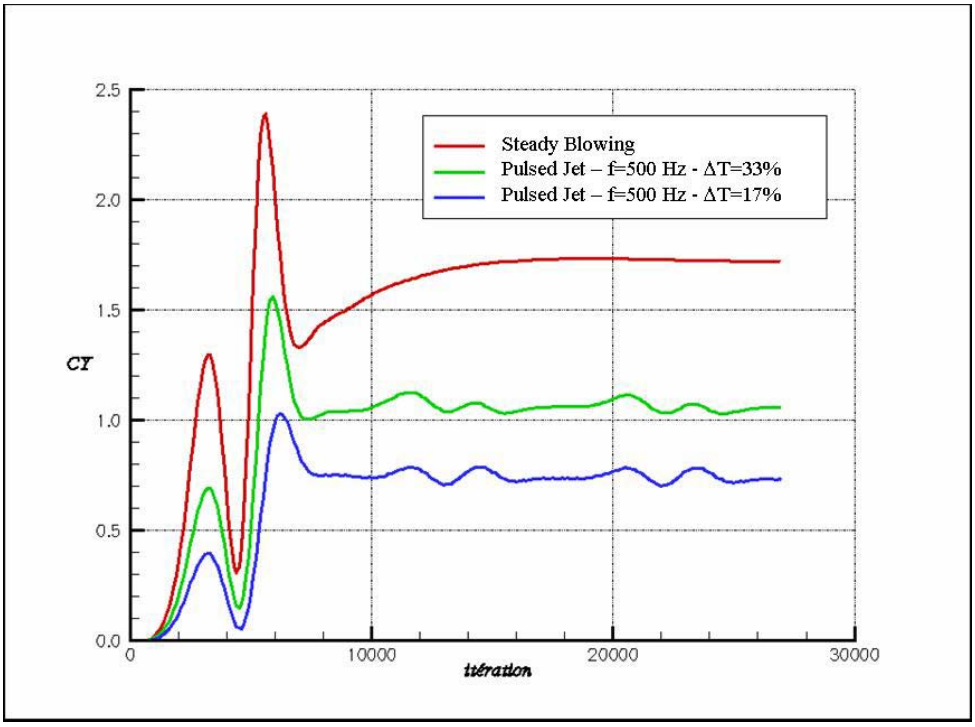

Figure 14 – Side force coefficient (pulsed jet effect)

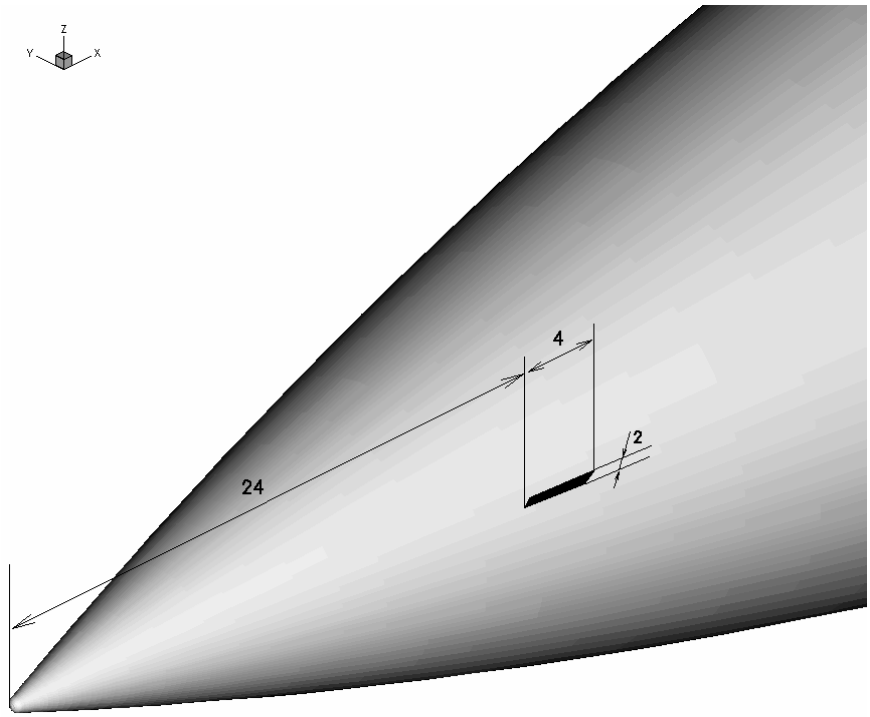

Figure 15 – Description of the DFE device

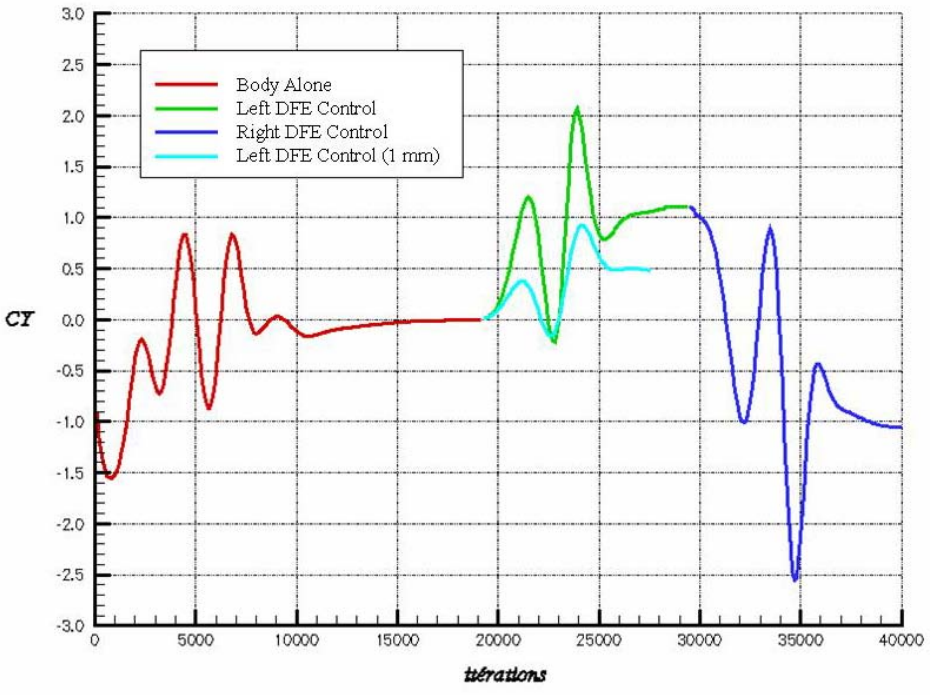

Figure 16 – Side force coefficient (DFE effect)

SYMPOSIA DISCUSSION – PAPER NO: 24

Discusser's Name: F Wong

Question:
Le nombre de Mach utilisè lors des tests de scufflerte était de l'ordre obe 0.1 à 0.2. Avey-vous utilise les vitesses plus hautes?

Author's Name: (P Champigny) P Denis

Author's Response:
Non, les essair our le fuselage litter Ont été realises jusq a Mach 0.35 et les essais futurs avec controle de lécoulemat ne déposserant pas Mach 0.2. Par centre, des études numériqes our le controle des tourbillans á plus haut nobre de Mach soet envisagée pour l'aveaur. (Mach supersonique entre autre)

This page has been deliberately left blank

Page intentionnellement blanche

ONERA

Numerical Simulation of Forebody Vortices at High Angle of Attack and their Control Using Innovative Systems

Authors : Pascal Denis, Sébastien Deck, Patrick Champigny

Office National d'Études
et de Recherches Aérospatiales
www.onera.fr

Numerical Simulation of Forebody Vortices at High Angle of Attack

Numerical Simulation of Forebody Vortices at High Angle of Attack

Garteur-AG42 ONERA test case

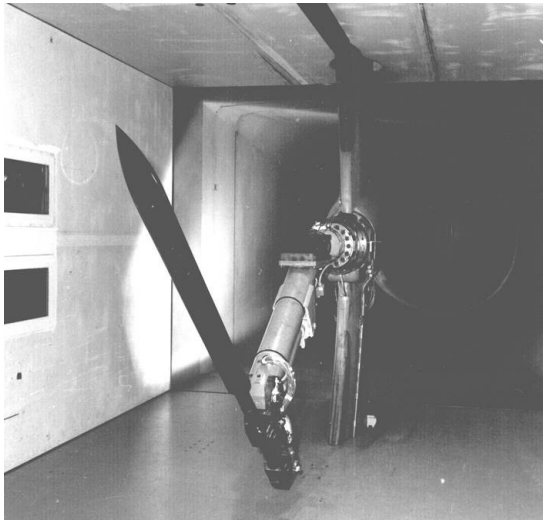

SKETCH OF PRESSURE-TAPPED MODEL

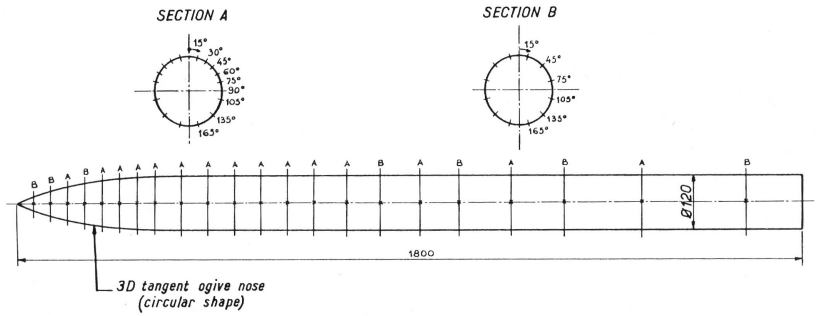

Model geometry

Diameter = 120 mm

Total length = 1800 mm (15D)

Ogive : 3D tangent ogive circular profile (R=1110 mm)

Flow conditions for the numerical test case

- Mach = 0.2
- Angle of attack = 45.43
- Stagnation pressure = 3.85 bars
- Stagnation temperature = 300 K
- Reynolds number ReD = 2.0 10^6
- Adiabatic wall
- Free transition
- Upstream turbulence level = 0.08%

ONERA

Numerical Simulation of Forebody Vortices at High Angle of Attack

Turbulence Modeling

1) SA turbulence model

$$\underbrace{\frac{\partial \tilde{\upsilon}}{\partial t} + \frac{\partial \tilde{u}_j \tilde{\upsilon}}{\partial x_j}}_{CONVECTION} = \underbrace{c_{b1}\tilde{S}\tilde{\upsilon}}_{PRODUCTION} + \frac{1}{\sigma}\underbrace{\left[\frac{\partial}{\partial x_j}\left((\upsilon+\tilde{\upsilon})\frac{\partial \tilde{\upsilon}}{\partial x_j}\right) + c_{b2}\frac{\partial \tilde{\upsilon}}{\partial x_j}\frac{\partial \tilde{\upsilon}}{\partial x_j}\right]}_{DIFFUSION} - \underbrace{c_{w1}f_w(r)\left(\frac{\tilde{\upsilon}}{d}\right)^2}_{DESTRUCTION}$$

2) SARC : SA+ rotation correction

$$\tilde{S}_{SARC} = \tilde{S}_{SA} + C_{vor}\min\left(0., |\Omega| - |S|\right) \qquad C_{vor} = 4$$

3) DES : combine the best features of RANS and LES

$$\tilde{d} = \min\left(d, C_{DES}\Delta\right) \qquad \text{with } \Delta \text{ computational mesh size}$$

- attached boundary layer : $\tilde{d} = d \longrightarrow \upsilon_t = \upsilon_t\big|_{SA}$
- far from walls : $\tilde{d} = C_{DES}\Delta \longrightarrow \upsilon_t \sim S\Delta^2$

Numerical Simulation of Forebody Vortices at High Angle of Attack

Grid

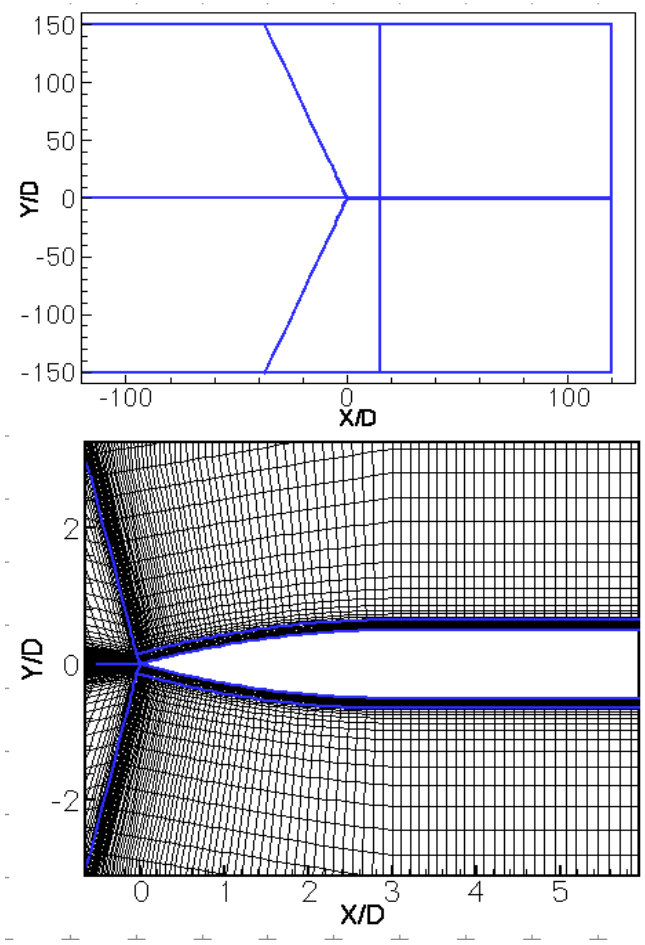

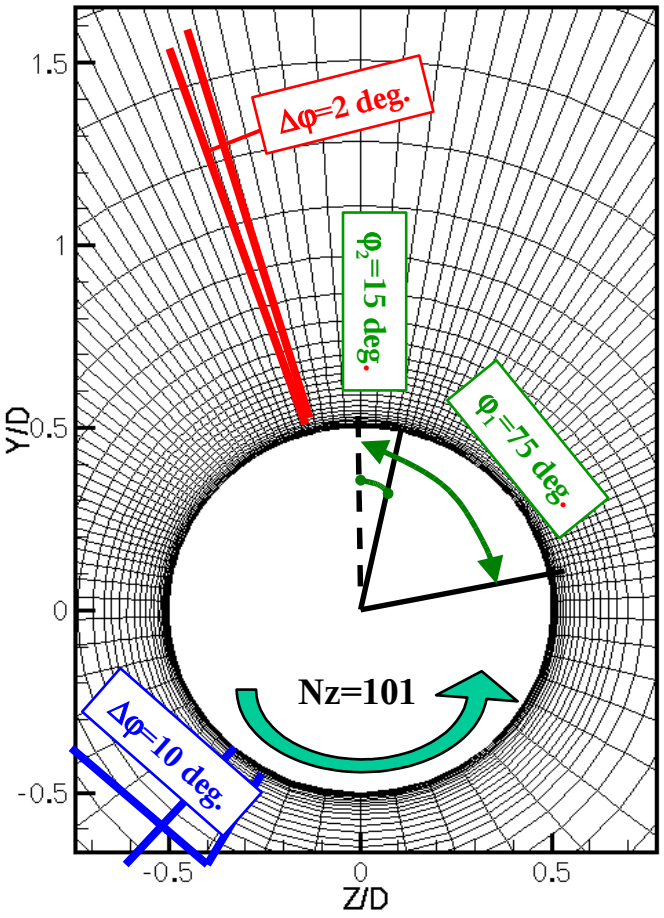

$N_{xyz}=2.10^6$

ONERA

Numerical Simulation of Forebody Vortices at High Angle of Attack

Convergence history

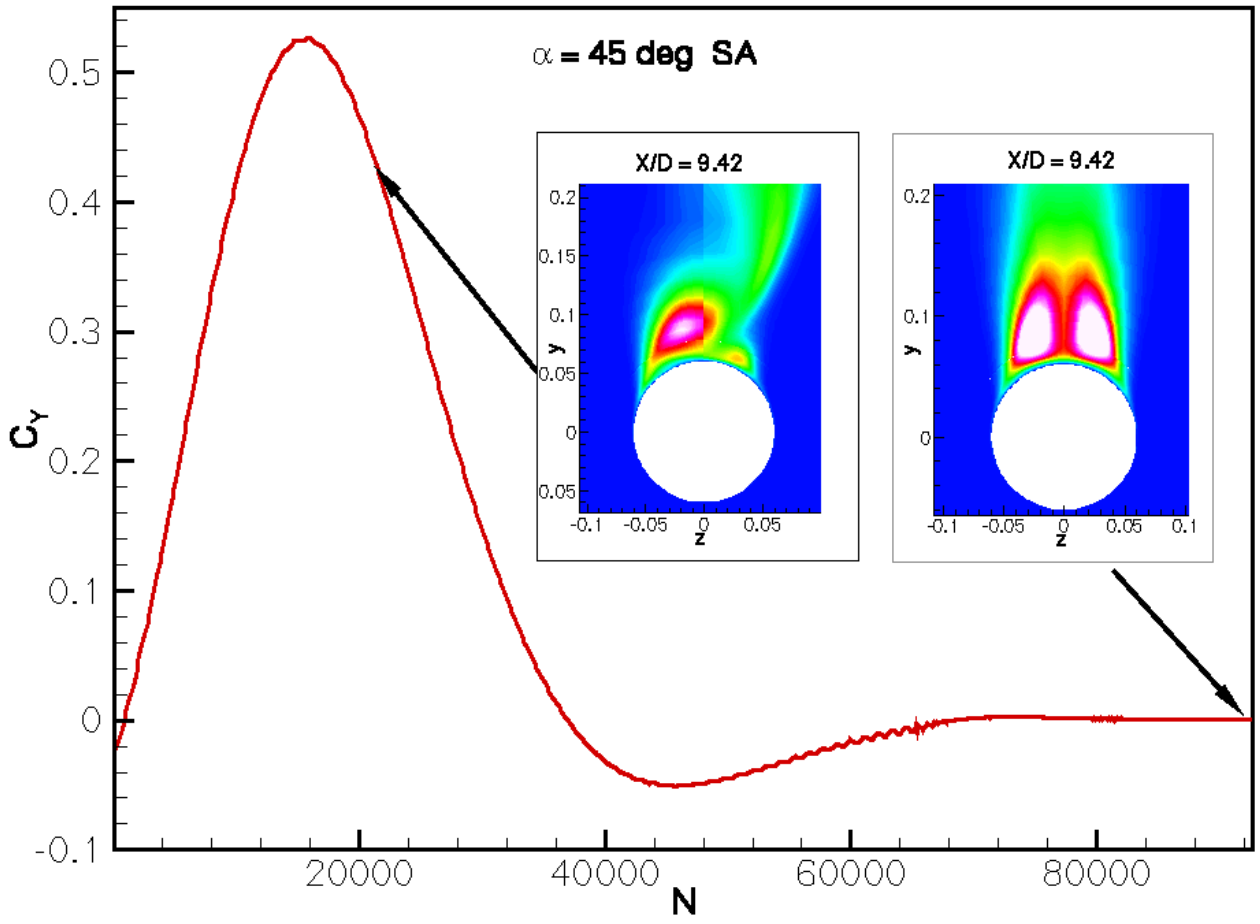

ONERA

Numerical Simulation of Forebody Vortices at High Angle of Attack

Effect of the turbulence model

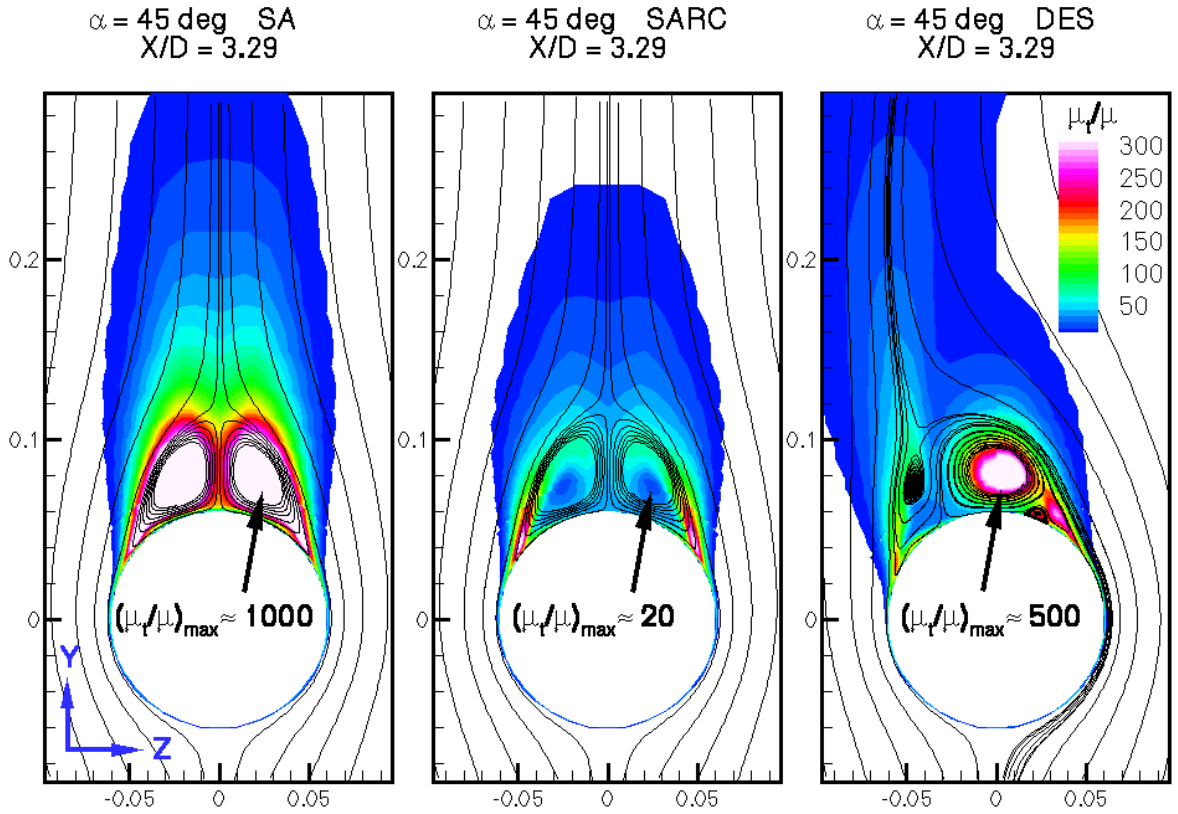

- No (weak) effect of rotation correction on the vortices (a)symmetry
- Asymmetrical vortices only reproduced by DES

ONERA

Numerical Simulation of Forebody Vortices at High Angle of Attack

Transverse Cp distributions*

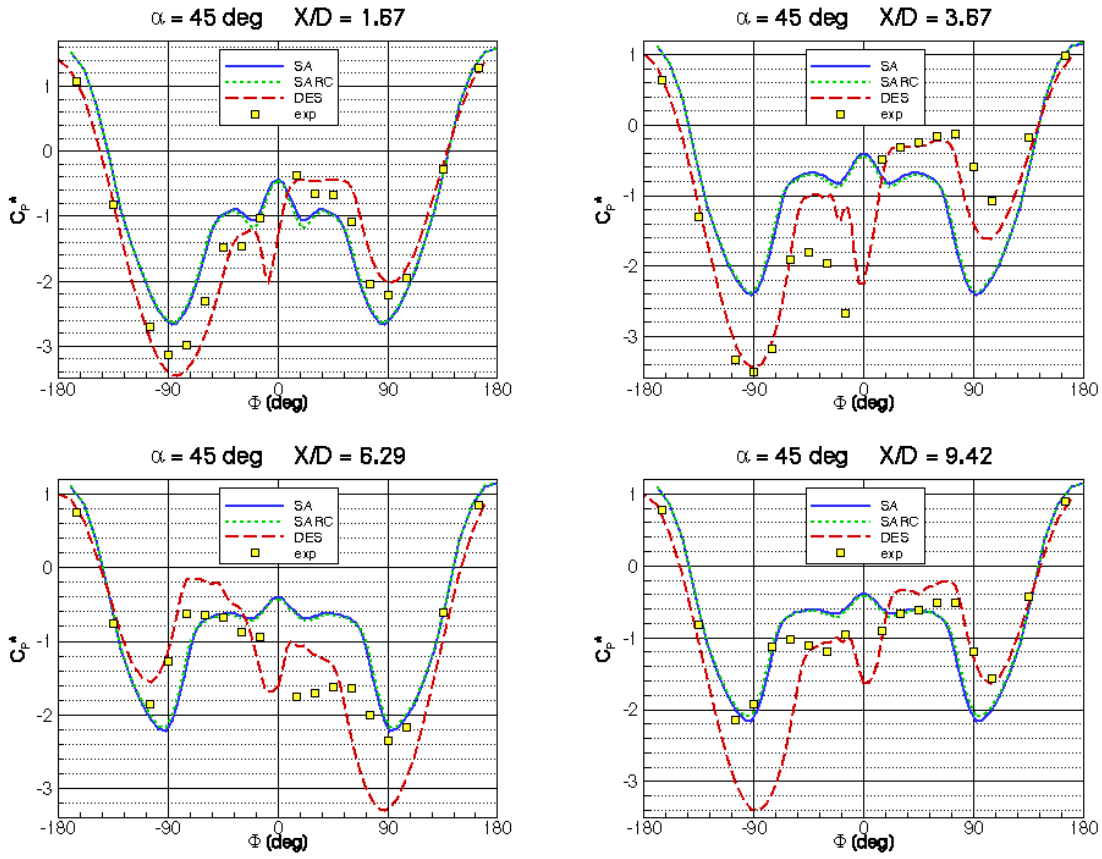

- Sign change of the asymmetry when going from the nose to the rear part
- Alternative shedding of the vortices on each side of the body

ONERA

Numerical Simulation of Forebody Vortices at High Angle of Attack

Local axial, normal and side force coefficients

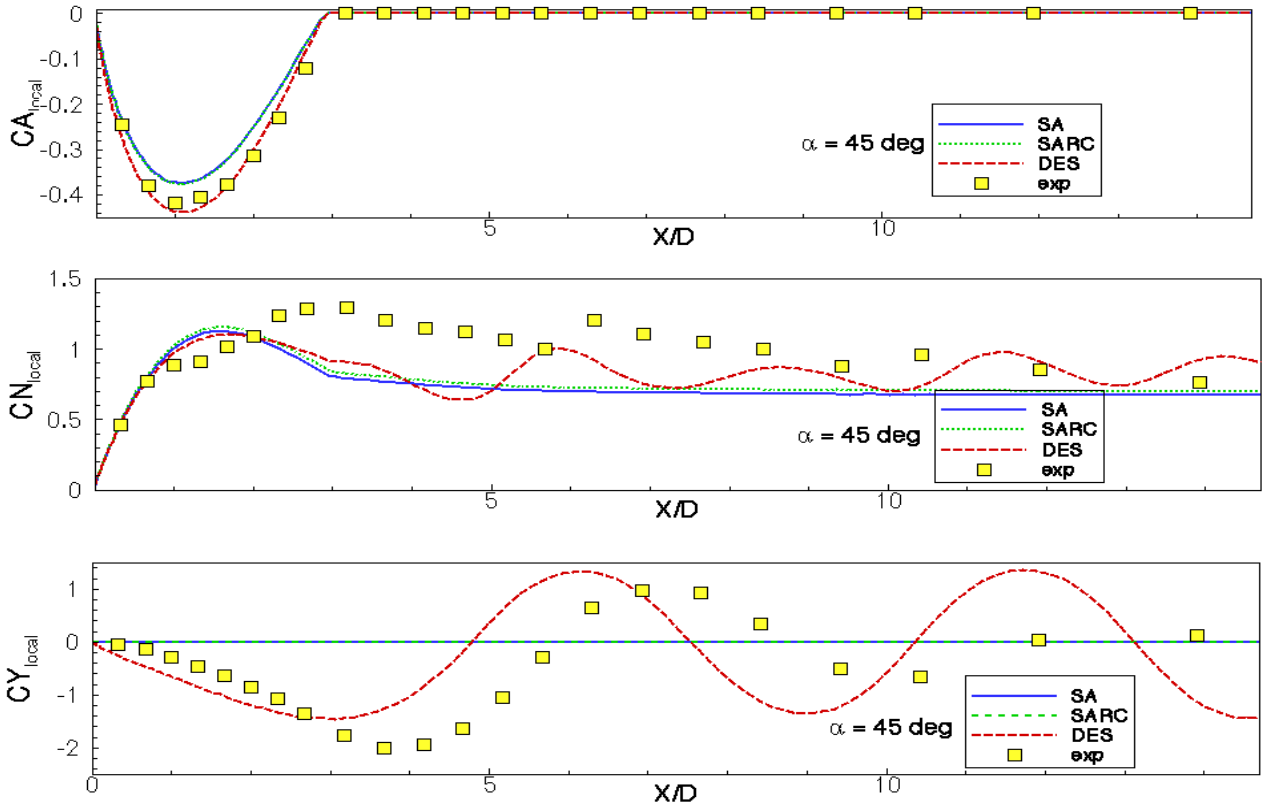

- The local side force is axially cyclic in nature
- Cy is not damped when going to the rear-part (base flow effect ?)

ONERA

Numerical Simulation of Forebody Vortices at High Angle of Attack

Time/space equivalence : 2D unsteady wake / 3D asymmetric vortex

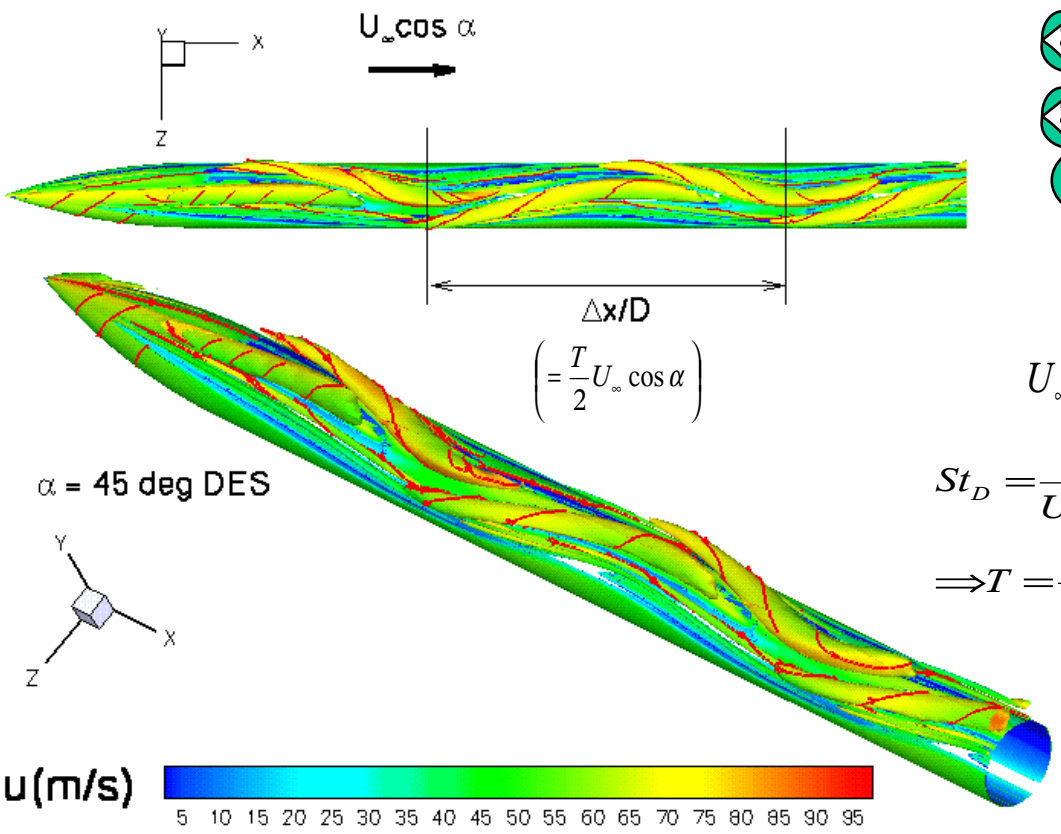

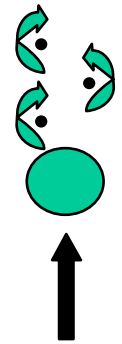

$U_\infty \sin\alpha$

$$\frac{\Delta x}{D} = \frac{1}{S\tan\alpha}$$

$S_{exp} = 0.21$
$S_{CFD} = 0.17$

$$St_D = \frac{f D}{U_\infty \sin\alpha}$$

$$\Rightarrow T = \frac{1}{f} = \frac{D}{St_D U_\infty \sin\alpha}$$

ONERA

Numerical Simulation of Forebody Vortices at High Angle of Attack

Conclusion

- Three modeling have been assessed (SA/SARC/DES) on a 2.10^6 nodes grid and compared with available data ($Cp^*(X/D,\phi)$, global and local force coefficients)

- SA and SARC yield symmetrical vortices (weak effect of RC) at convergence
  ⇒ Necessity to provide a time-history convergence for Cy

- Asymmetry has been successfully recovered by DES
  ⇒ stable and steady in time
  ⇒ Time/space equivalence well reproduced
  ⇒ wind-tunnel side-walls effects are not the driving phenomenon
  ⇒ unlike experiment, computed Cy is not damped

Forebody Vortices Control at High Angle of Attack

Forebody Vortices Control at High Angle of Attack

Objectives

- **Controlling the forebody vortices at high angle of attack to :**
  - Cancel the side forces induced by the natural asymmetric flowfield
  - Participate to the missile piloting
- **Defining the actuator used for the future wind tunnel test (Continuous, pulsed jets or DFE)**

Forebody Vortices Control at High Angle of Attack

Configuration and Numerical Code

- **« Tangent Ogive cylinder body» fixed by wind tunnel facility :**
  - Model : D=0,04m ; L=13D ; λ_{ogive}=3 et r/D=0,01mm
  - Test case conditions : M_o=0,1 ; $\alpha \geq 30°$; P_i=1 bar ; T_i=298 K

    $\Rightarrow Re_D \cong$ $0{,}94.10^5$ (laminar flow)

- **Flu3m Code**
  - Unsteady computation ($\Delta t=5.10^{-6}$s / first order)
  - Roe flux ; Minmod limiter
  - Boundary condition for jet simulation

Forebody Vortices Control at High Angle of Attack

Mesh Description

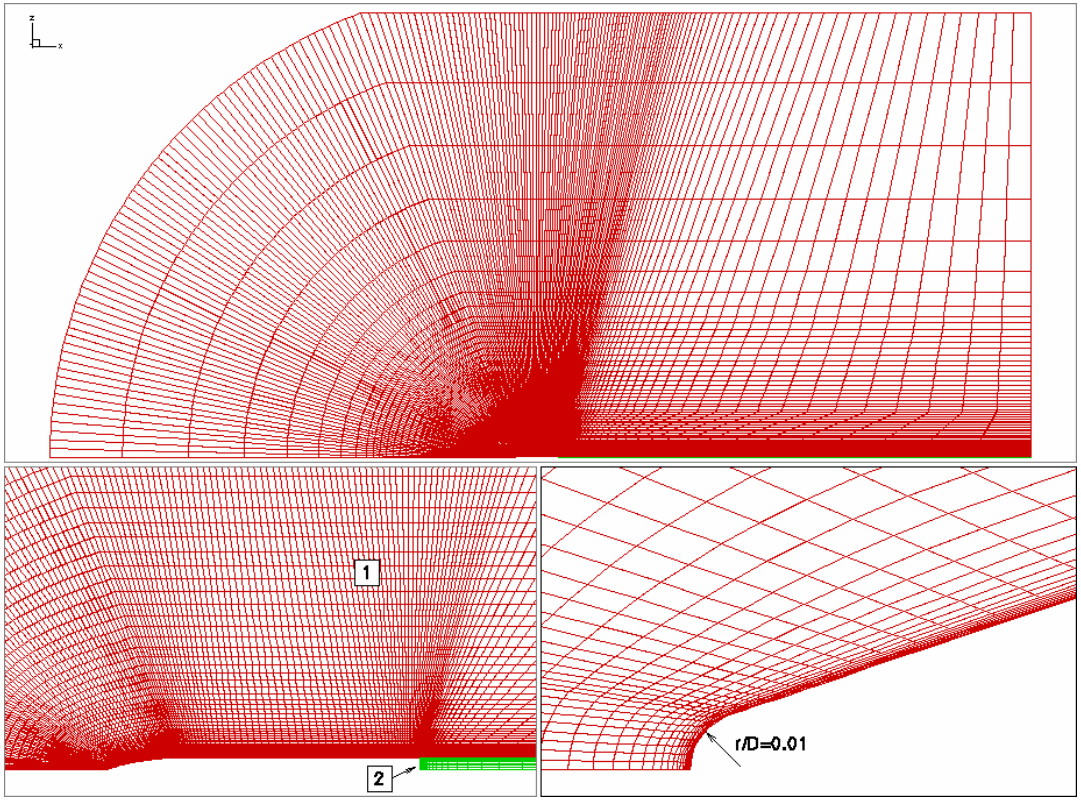

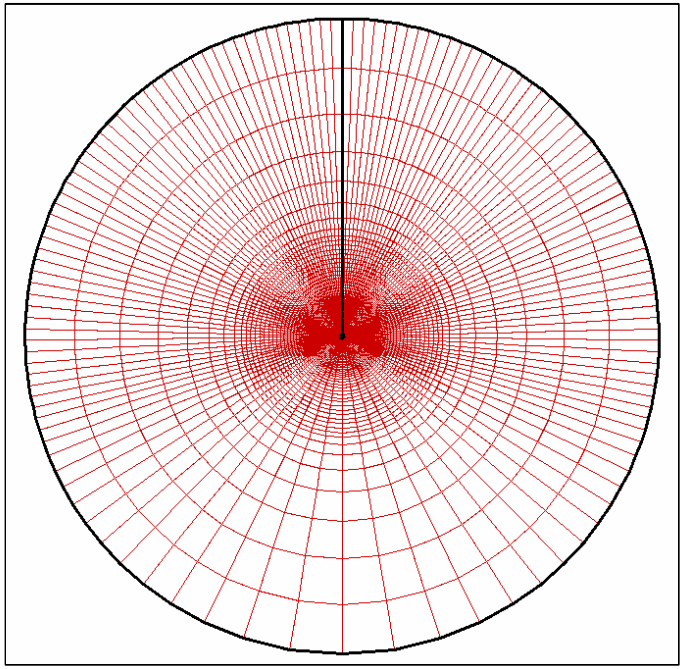

≈ 3 000 000 nodes (2 domains)

ONERA

Forebody Vortices Control at High Angle of Attack

Results without Control (Flow visualization)

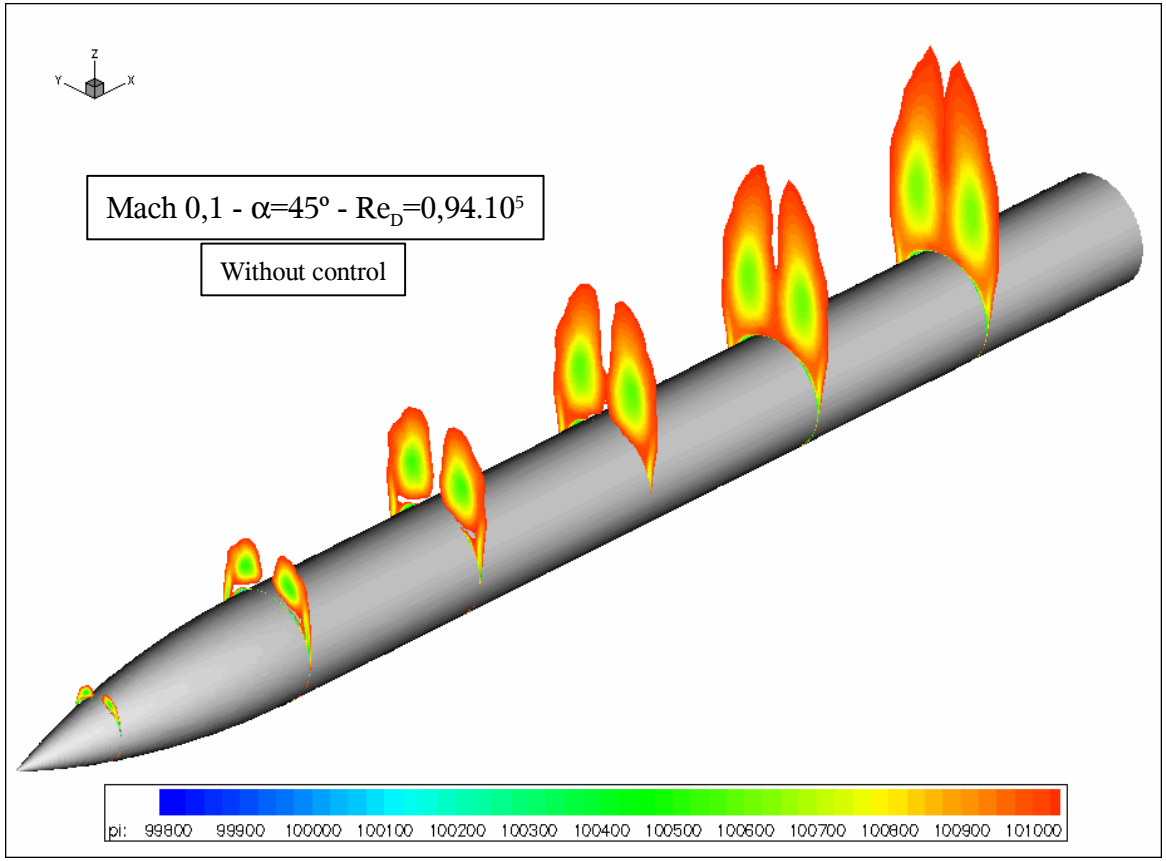

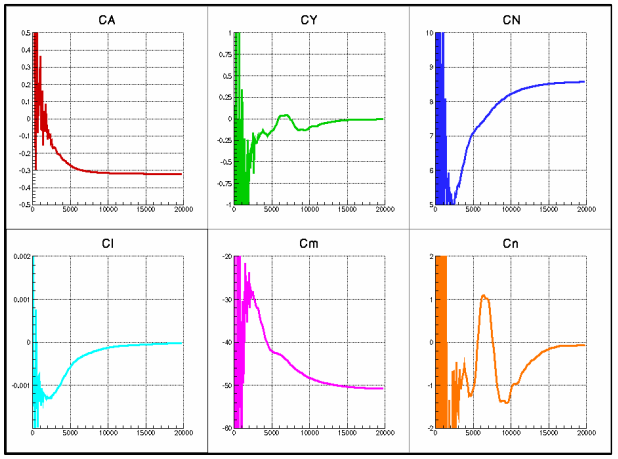

Convergence : ≈ 20 000 iterations

Symmetric flow (∀α)

ONERA

Forebody Vortices Control at High Angle of Attack

Results without Control (Experiment)

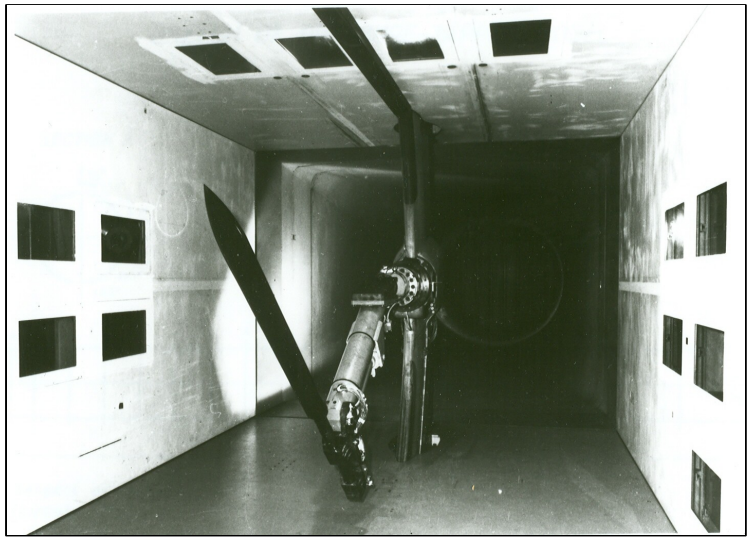

Model mounting in the ONERA F1 wind tunnel

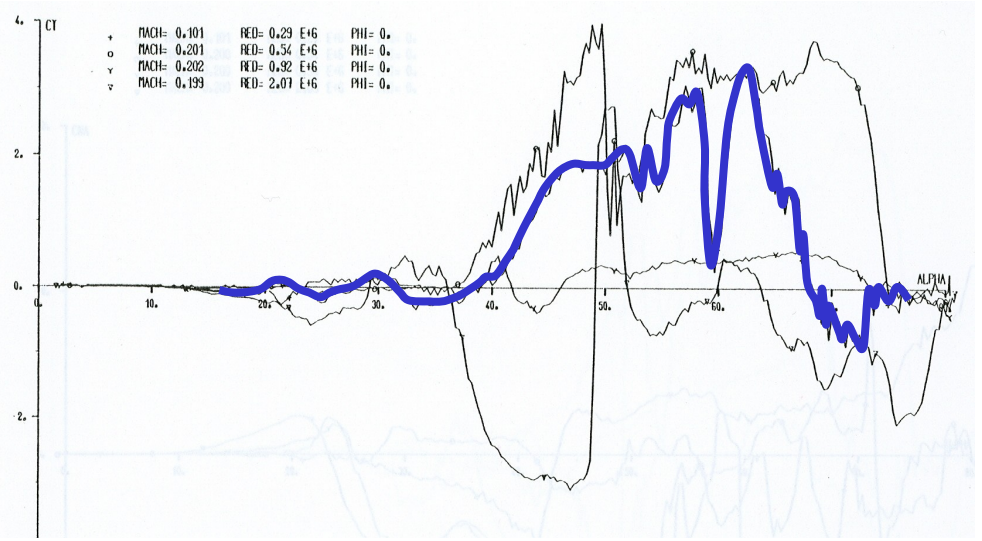

Evolution of the side force coefficient

ONERA

Forebody Vortices Control at High Angle of Attack

Jet Control (Description)

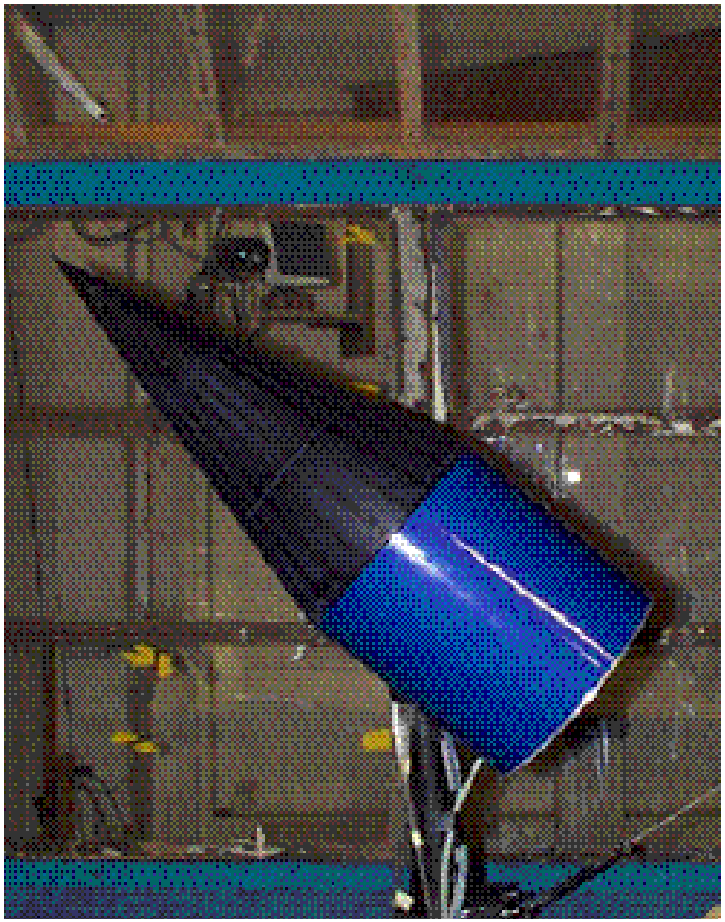

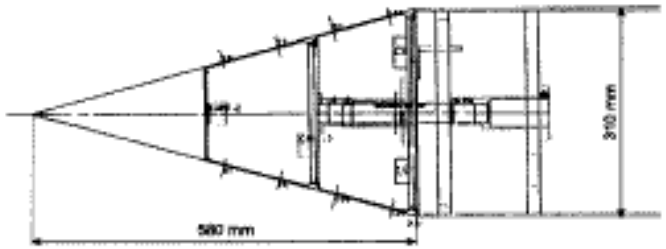

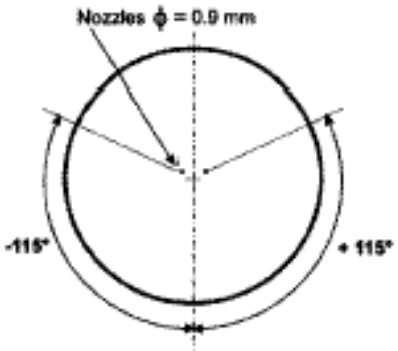

⇒ Based on Conical Ogive results from ONERA L1 wind tunnel test

ONERA

Forebody Vortices Control at High Angle of Attack

Jet Control (Description)

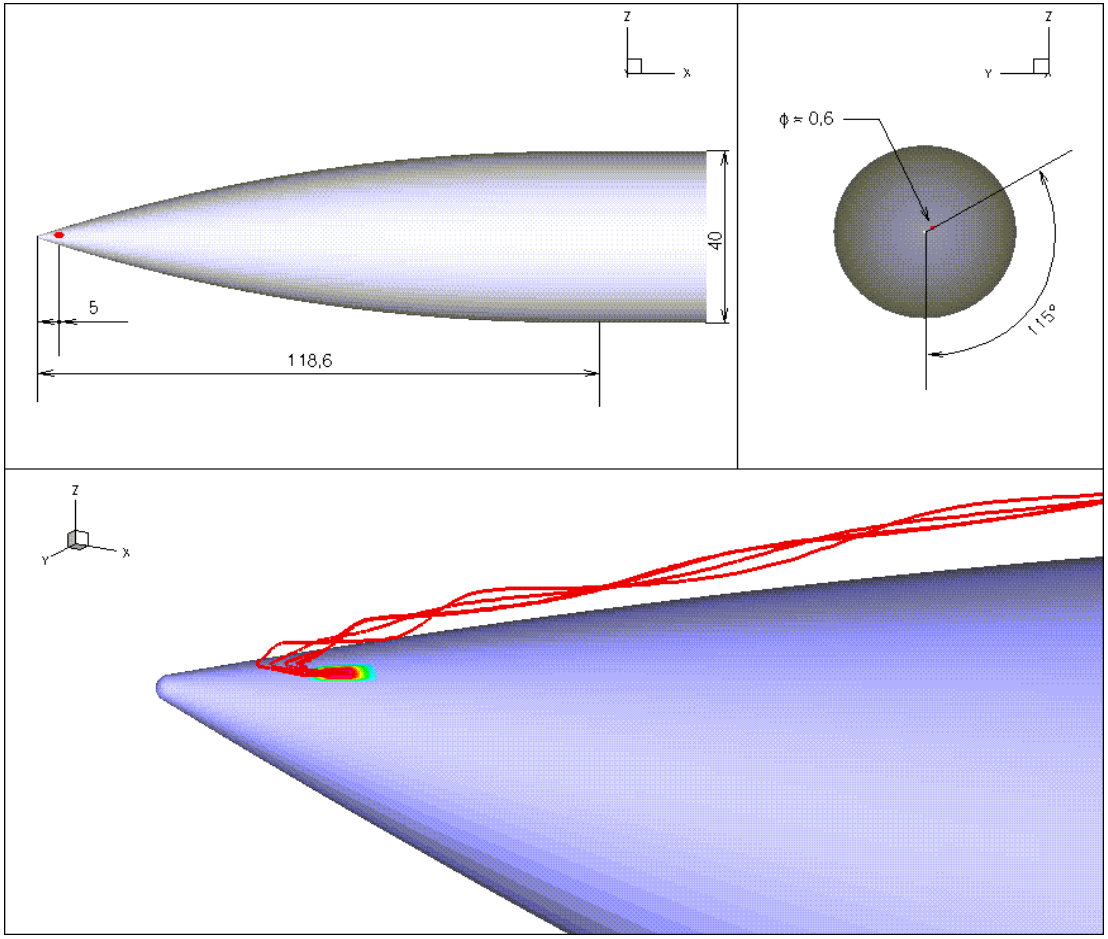

- Steady blowing / Pulsed jet
- Axial body axis injection
- $V_{jet} \approx 60 m/s$
- $q_{jet} \approx 0{,}02 g/s$
- $C_{\mu} \approx 2.10^{-3}$ $\left(= \dfrac{\dot{m}}{\rho_{\infty} V_{\infty} S_{ref}} \right)$

ONERA

Forebody Vortices Control at High Angle of Attack

Jet Control (Flow visualization)

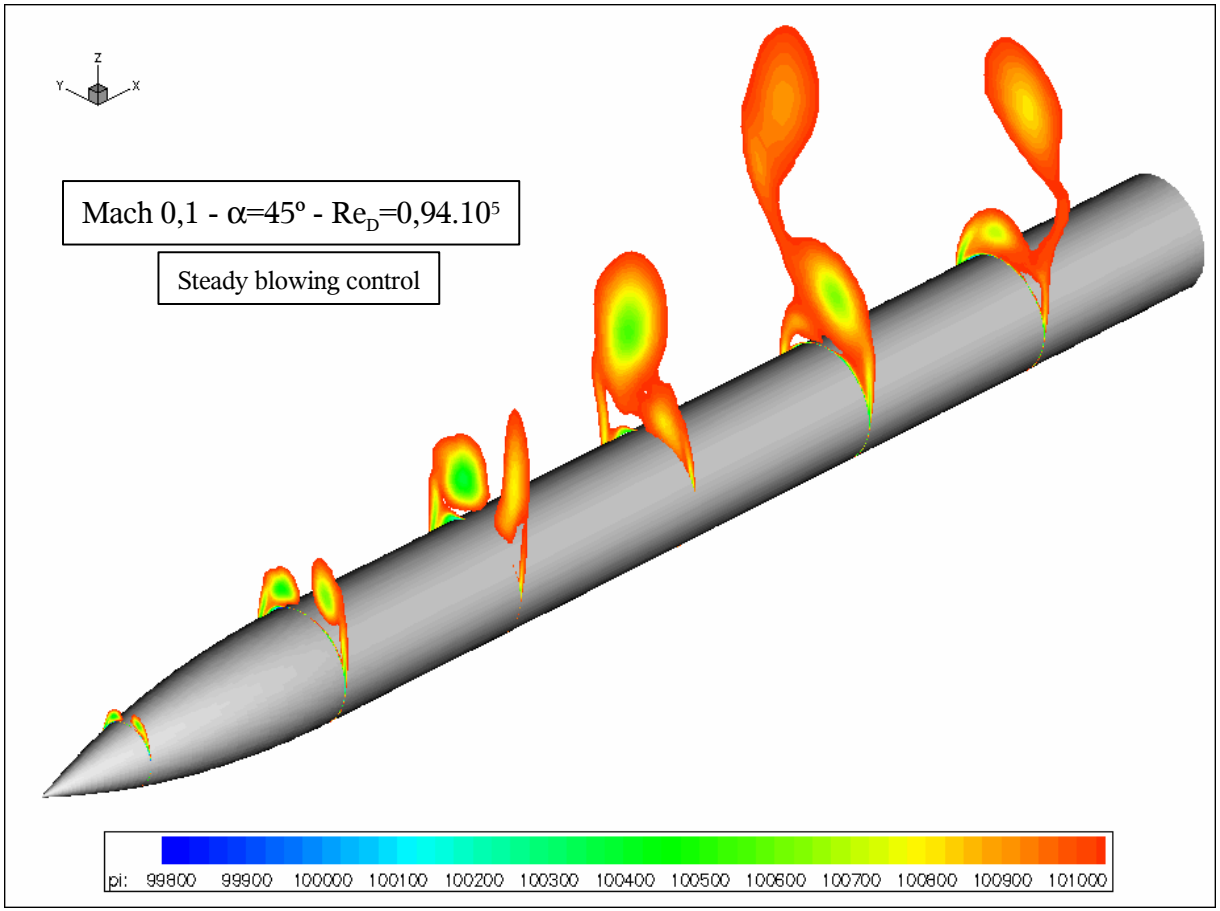

M=0,1 / α=45°	CL	Cd	CY
Without control	8,51	-0,322	0
With control	10,42	-0.307	1,75
Experiment	10,65	-0,279	1,58

ONERA

Forebody Vortices Control at High Angle of Attack

Jet Control (Q criteria)

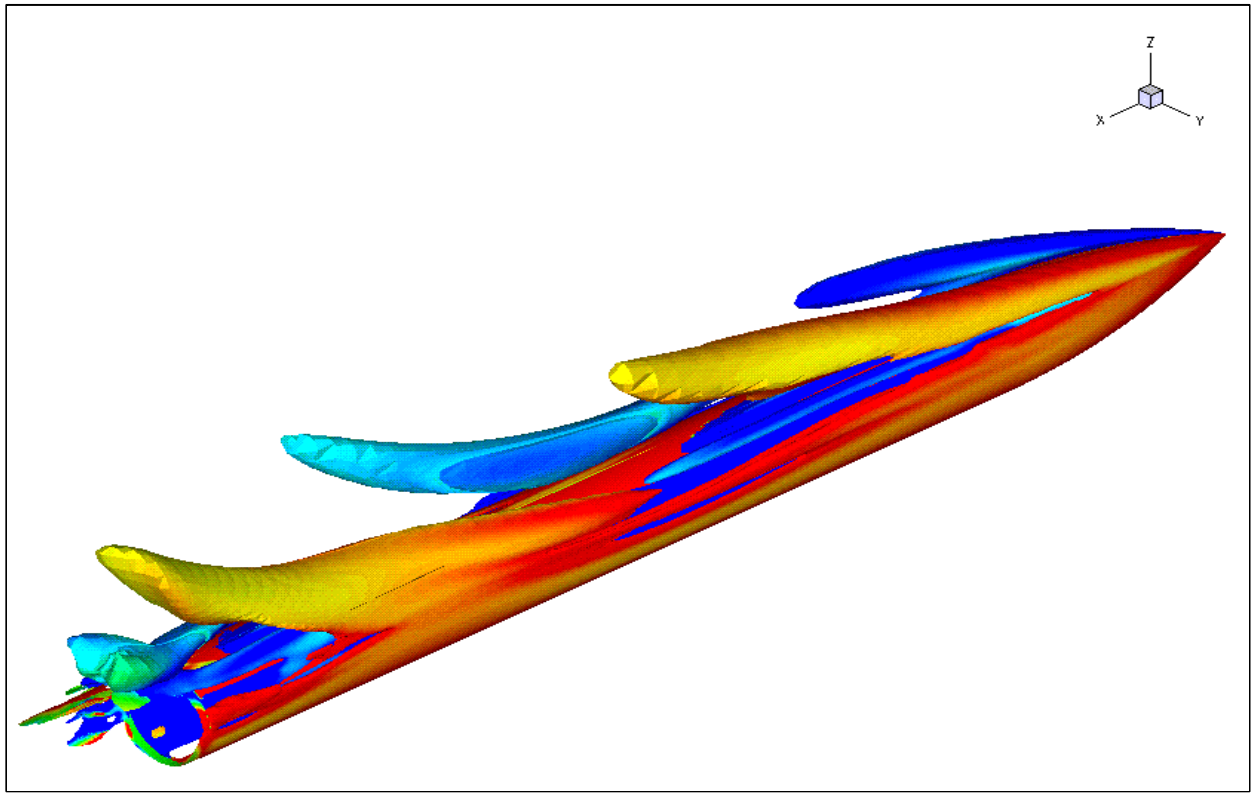

$$Q = \frac{1}{2}\left(\|\Omega\|^2 - \|S\|^2\right)$$
$$and\ Q > 0$$

Iso-Q map, colored with the longitudinal vorticity (Q=1)

ONERA

Forebody Vortices Control at High Angle of Attack

Jet Control (Friction lines)

Experimental side view (α=45°)

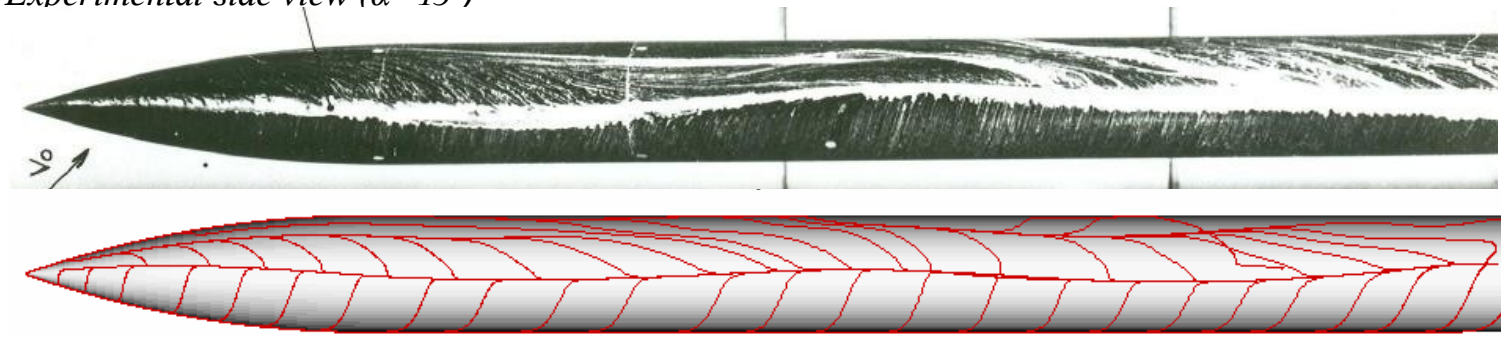

Numerical side view (α=45°)

Experimental top view (α=45°)

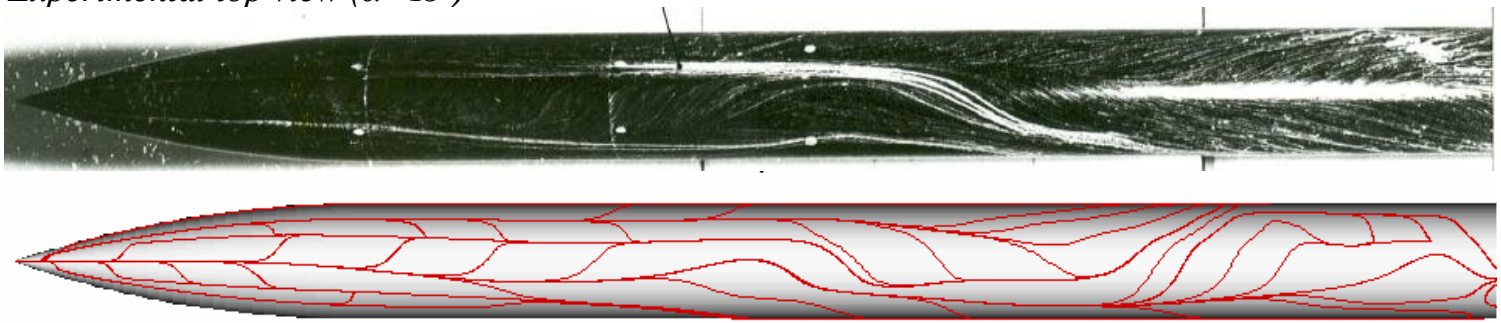

Numerical top view (α=45°)

ONERA

Forebody Vortices Control at High Angle of Attack

Jet Control (Side force evolution)

Side Force Coefficient

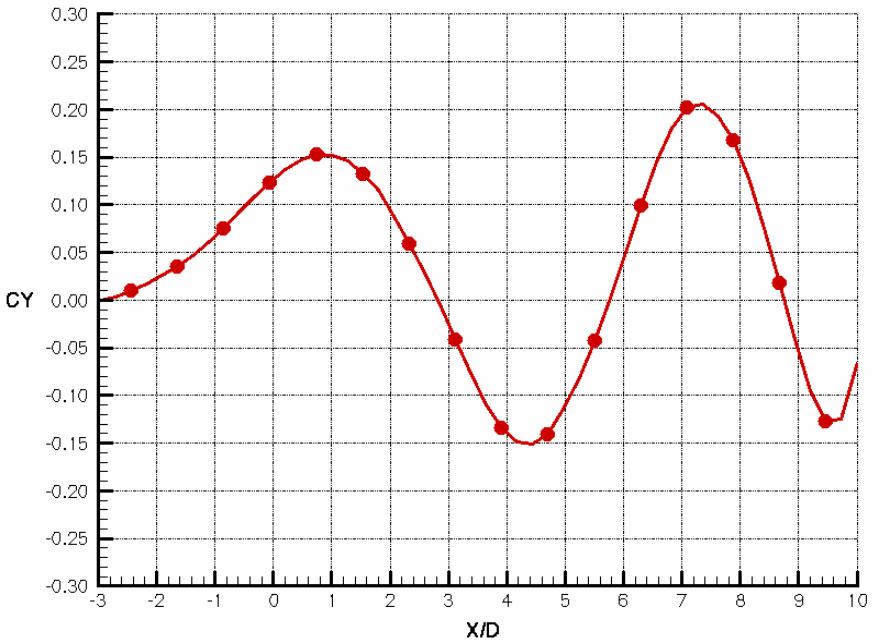

Cumulative Side Force Coefficient

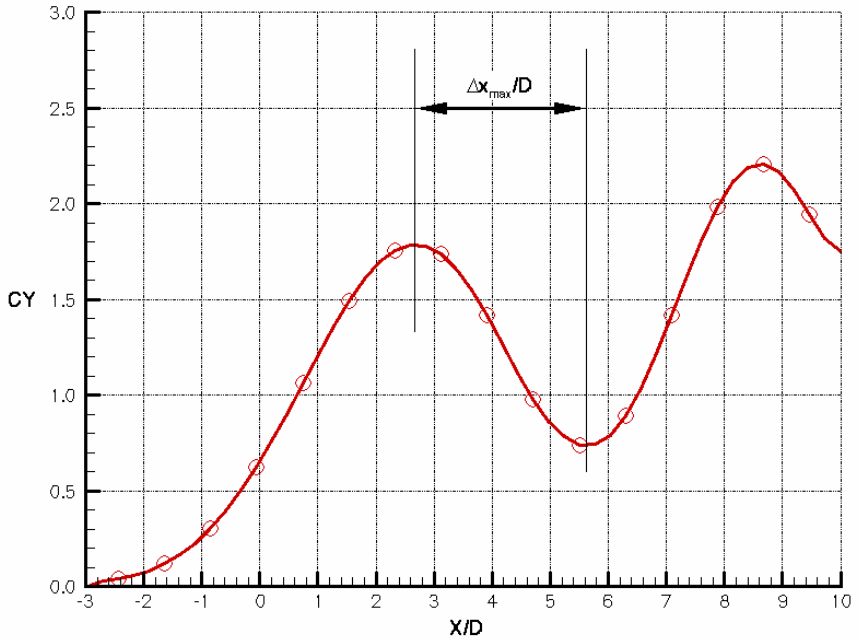

$$S_t = \frac{1}{2\left(\frac{\Delta x_{max}}{D}\right)\tan\alpha} \quad \Rightarrow \quad S_t \approx 0{,}17 \quad (\text{and } S_{t\ exp} \approx 0{,}21)$$

ONERA

Forebody Vortices Control at High Angle of Attack

Jet Control (Side force)

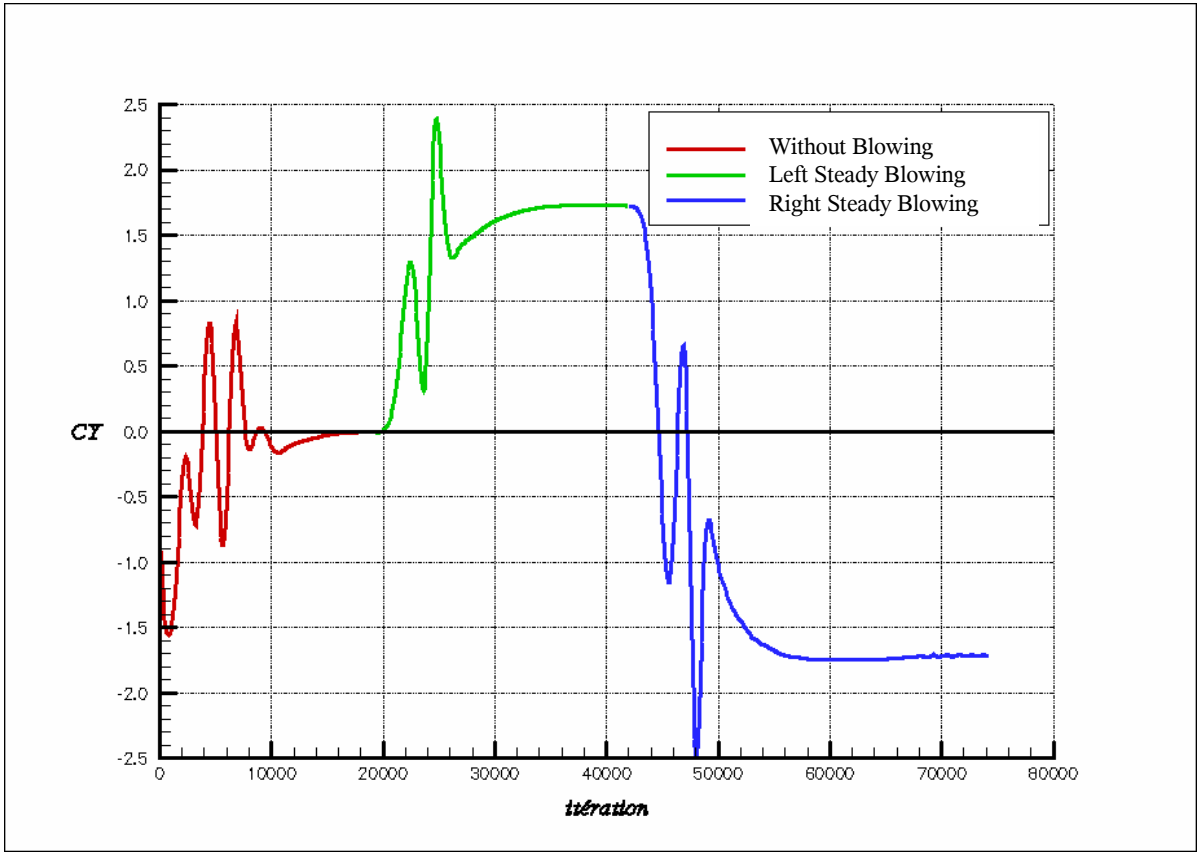

Side Force (α=45°)

- Efficient control

- Perfectly symmetrical effect (« left/right »)

ONERA

Forebody Vortices Control at High Angle of Attack

Jet Control (Cμ effect)

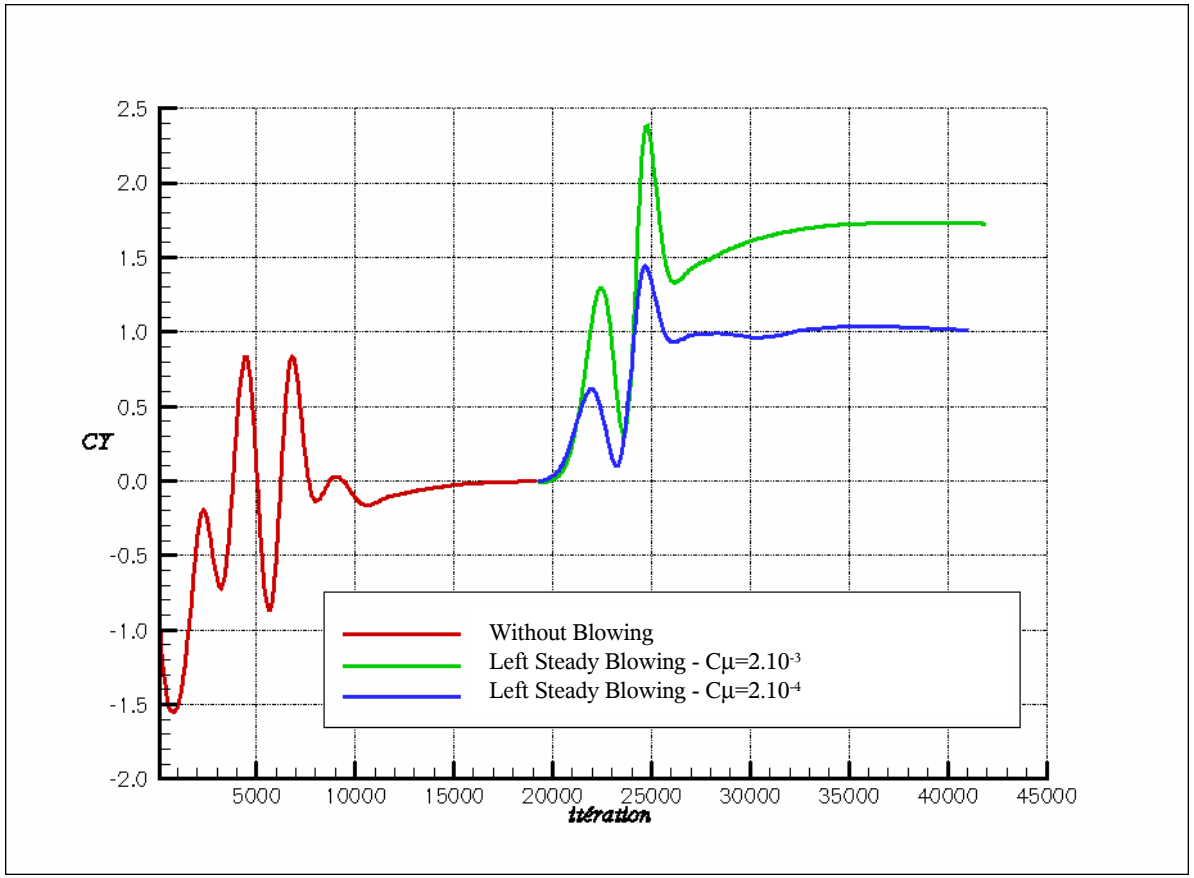

Side Force (α=45°)

$V_{jet} \approx 20 m/s$

$q_{jet} \approx 0{,}007 g/s$

$\Downarrow$

$C\mu \approx 2.10^{-4}$

$\Downarrow$

Maintenance of control

ONERA

Forebody Vortices Control at High Angle of Attack

Jet Control (Pulsed jet)

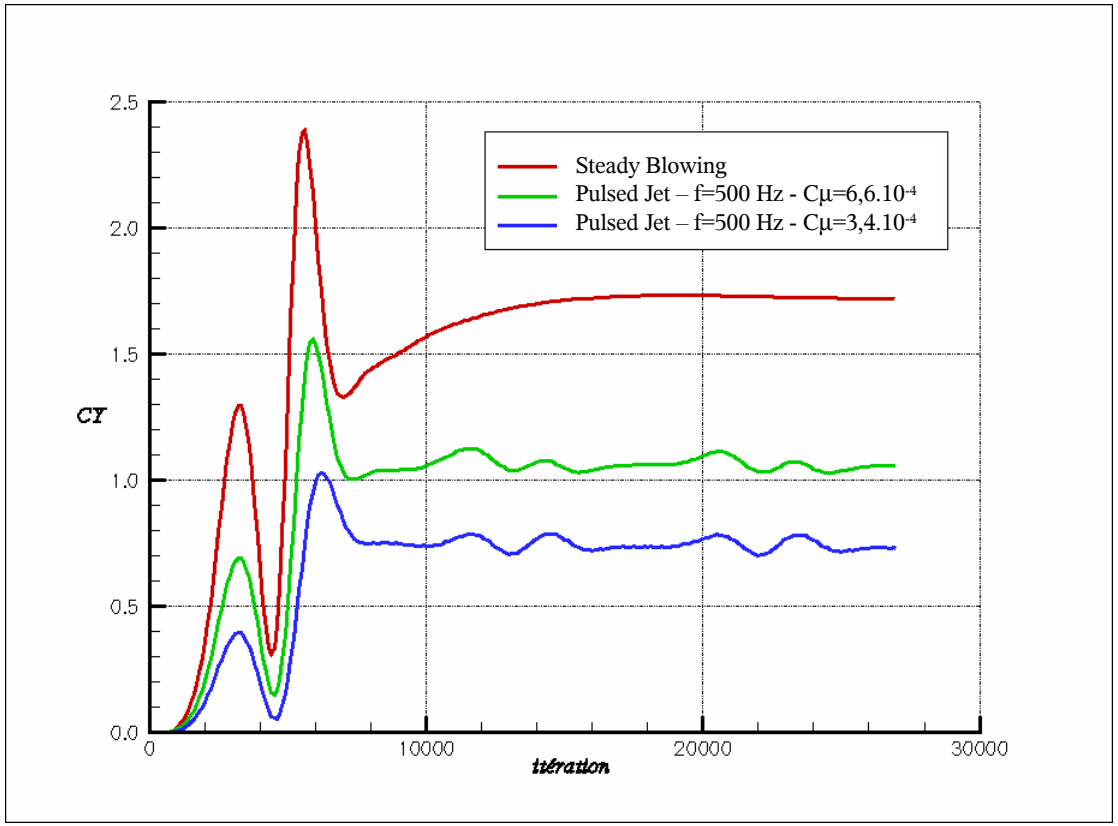

Side Force (α=45°)

Jet frequency : f=500 Hz

- Side force can be obtained with pulsed jet
- Side force is dependant on the mass flow jet
- For equivalent mass flow, same side force with pulsed jet or steady blowing control

ONERA

Forebody Vortices Control at High Angle of Attack

Jet Control (Angle of attack effect)

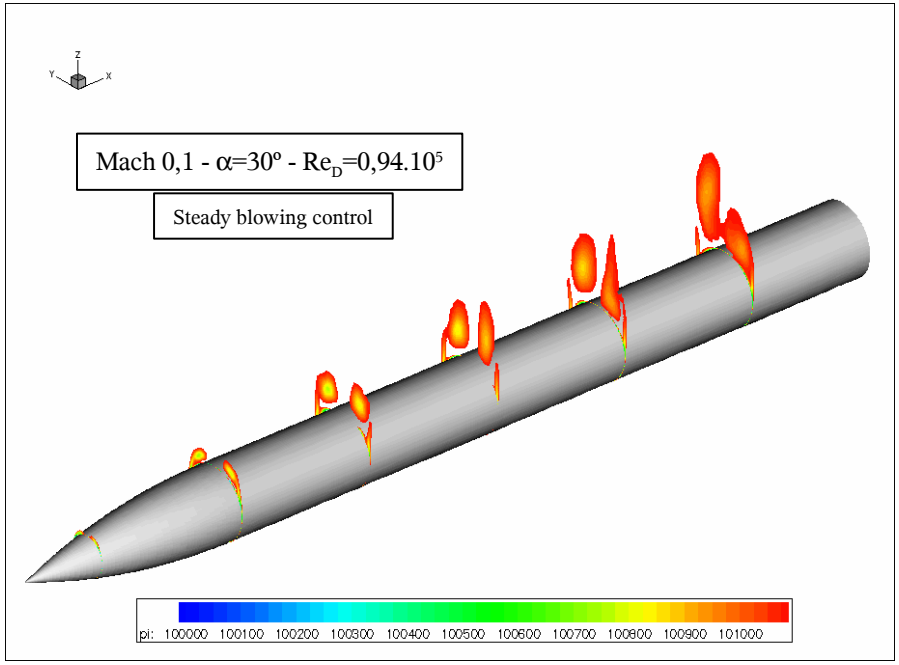

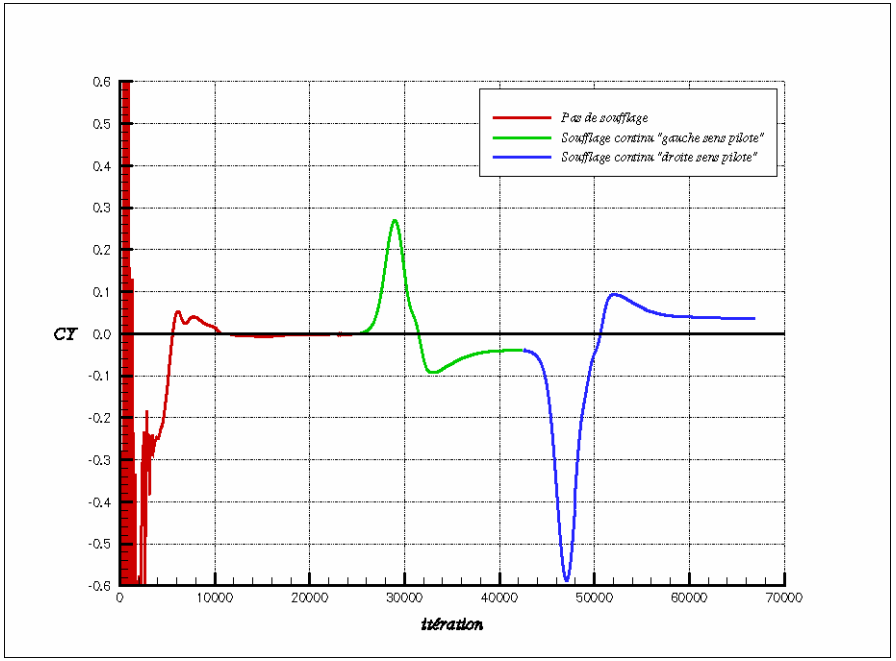

⇒ Low control efficiency

ONERA

Forebody Vortices Control at High Angle of Attack

Jet Control (Angle of attack effect)

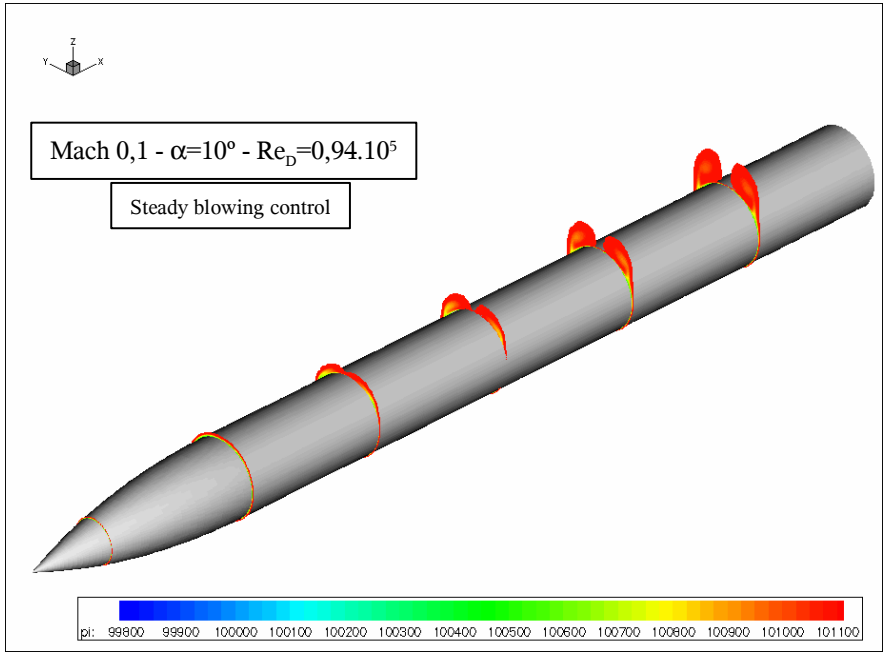

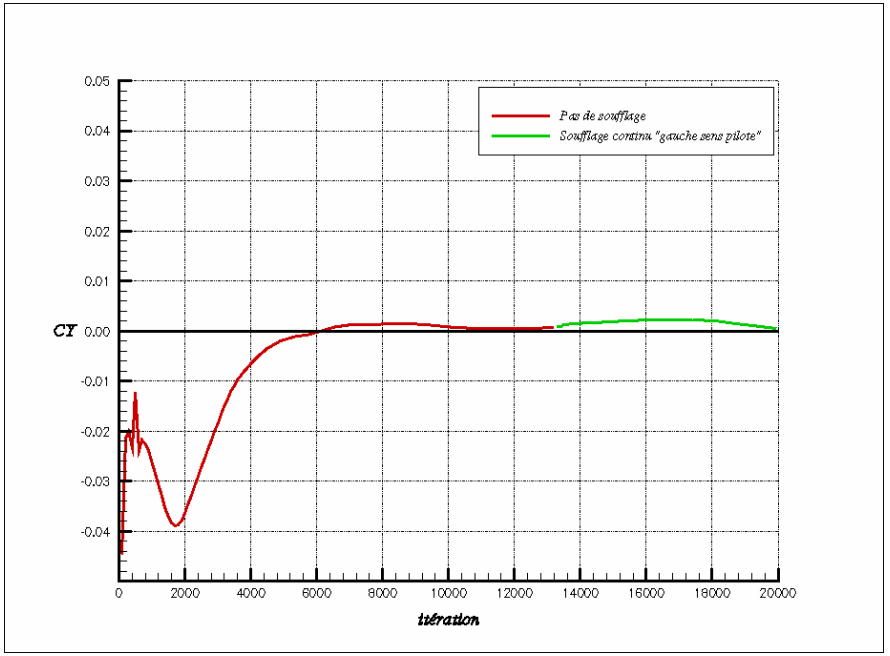

⇒ No efficiency

ONERA

Forebody Vortices Control at High Angle of Attack

DFE Control (Description)

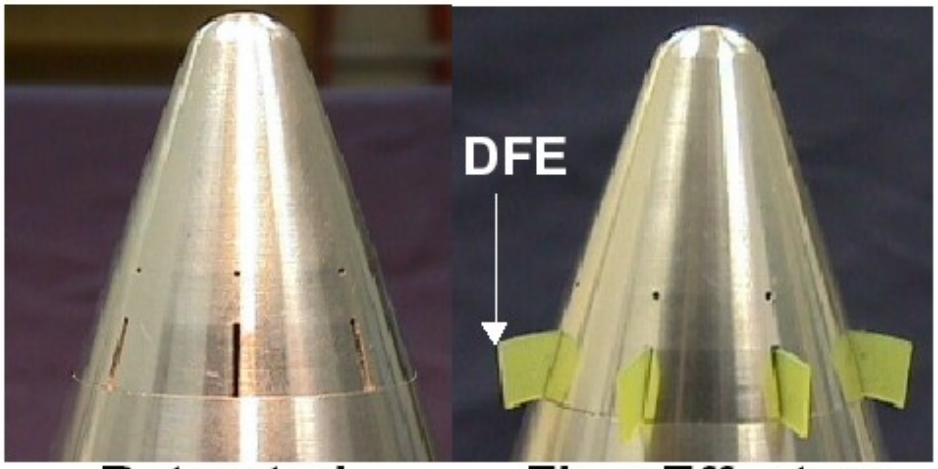

$\Rightarrow$ Based on DFE Orbital design

ONERA

Forebody Vortices Control at High Angle of Attack

DFE Control (Description)

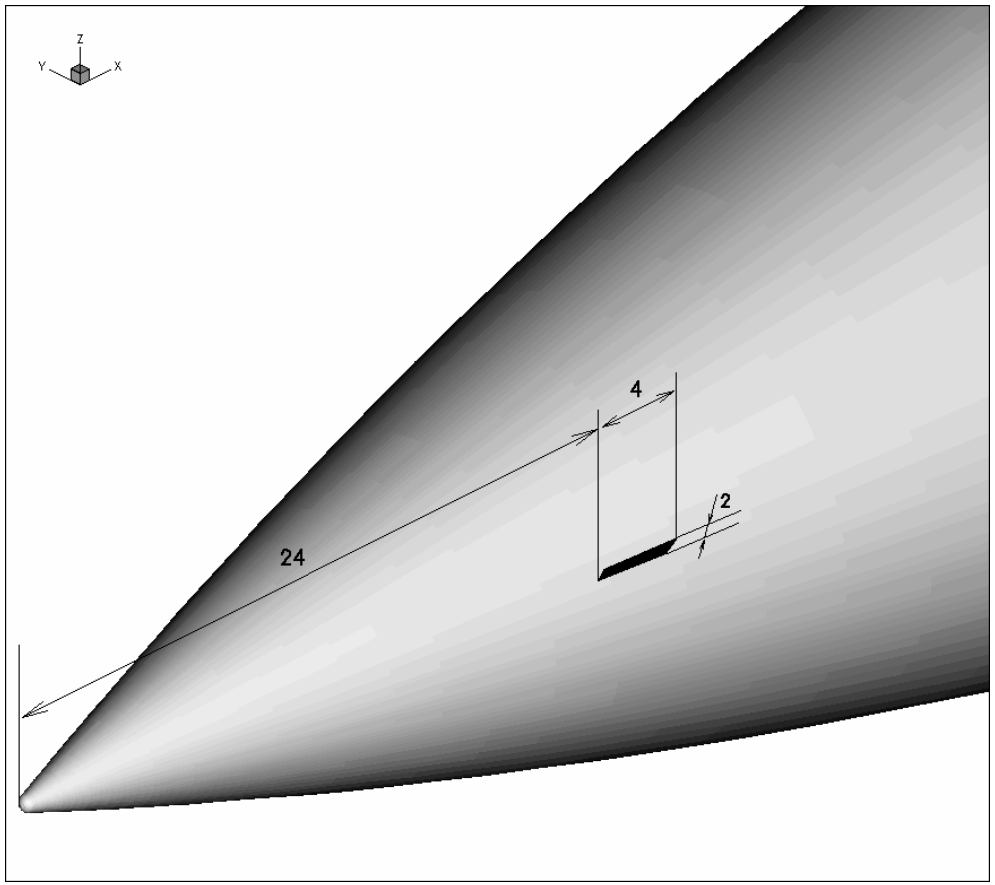

DFE Modelisation

- boundary condition
- no thickness surface

Two heights : 2 and 1 mm

ONERA

Forebody Vortices Control at High Angle of Attack

DFE Control

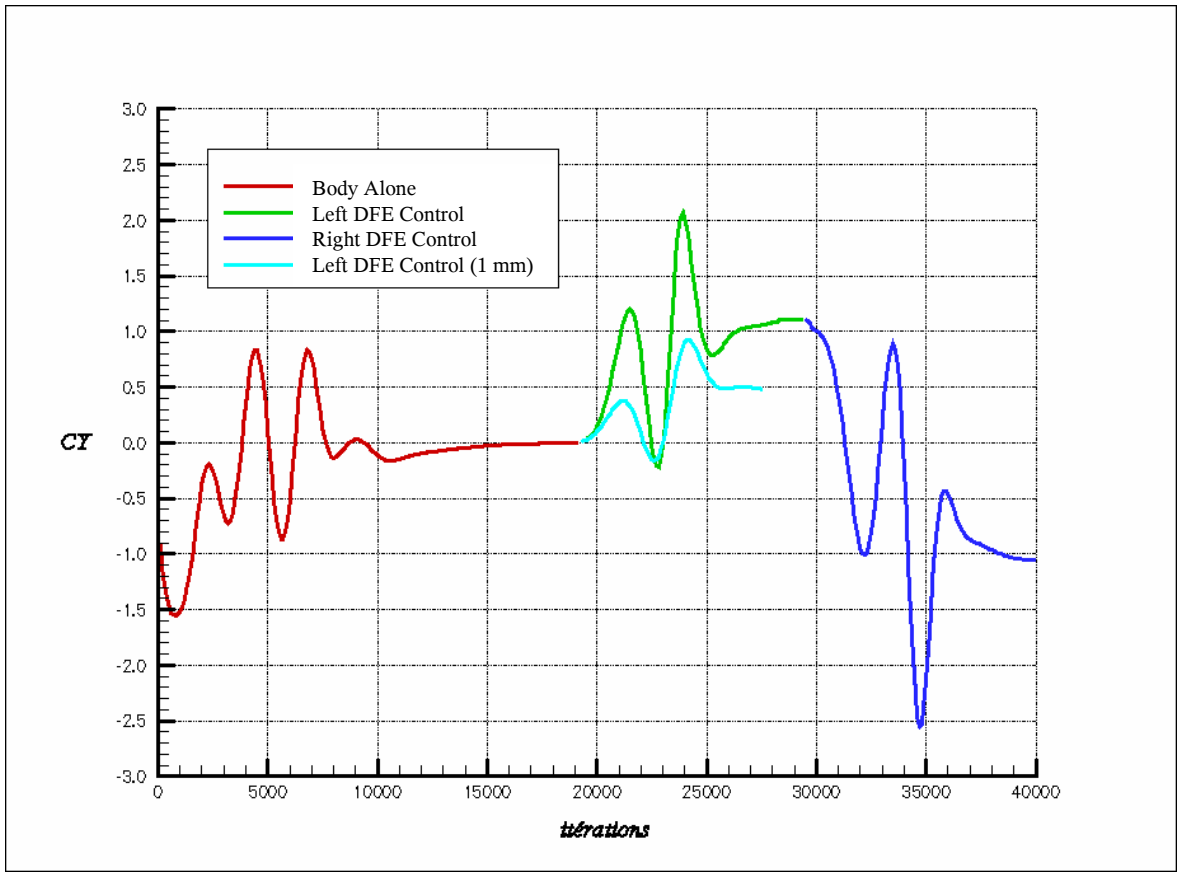

- Side force can be generated and controlled by DFE actuator

- DFE height reduction leads to a decrease of the control efficiency

ONERA

Forebody Vortices Control at High Angle of Attack

Conclusion

- **Numerical simulations have shown that forebody vortices at high angle of attack can be controlled by :**
  - Steady Blowing ;
  - Pulsed jet ;
  - DFE.

- **Nevertheless, their efficiency is limited to the high alpha range (i.e. greater than 30°)**

Perspectives

Numerical simulations of forebody vortices at high α

- Future work will focus on a deeper analysis of the flow field rather than on evaluating Side-Wall Effects (SWE) since the asymmetry has been reproduced without SWE
- A finer grid (e.g. suited for DES !) will be designed ⇒ better capture of the vortex sheet departure (possible unsteady phenomena ?)
- Evaluation of possible base flow effects ⇒ Damping of the side force coefficient

Forebody vortices control at high α

- Manufacture the control systems (use MEMS)
- Wind tunnel tests